DISTINCT ELEMENT SIMULATION OF MUSHY-STATE FORMING

Masaaki OTSU

January 1998

DISTINCT ELEMENT SIMULATION OF MUSHY-STATE FORMING

Masaaki OTSU

Department of Mechanical Engineering
Faculty of Engineering Science
Osaka University
Japan

ACKNOWLEDGEMENTS

The author sincerely acknowledges his indebtedness to Dr. Kozo Osakada, Professor of the Faculty of Engineering Science, Osaka University, for his continuous guidance and encouragement throughout this study. The author learned a lot from him about what to study and how to study.

The author's special thanks go to Dr. Takao Yoshikawa and Dr. Keiji Ogura, Professors of the Faculty of Engineering Science, Osaka University. They made many critical comments to the manuscript of this dissertation.

Great acknowledgements are also made to Dr. Ken-ichiro Mori, Professor of the Department of Production Systems Engineering, Toyohashi University of Technology, for his continuous guidance and valuable discussions throughout this study.

The author is grateful to Dr. Masanori Shiomi, Research Assistant of Osaka University and Mr. Shinji Hanami, Technician of Osaka University for their valuable suggestions and help during this study.

The author wishes to express his sincere gratitude to Dr. Karl F. MacDorman, Lecturer of Osaka University, for his dedicated revision and constructive criticisms of the manuscript of this dissertation.

The author's thanks are also given to Mr. T. Wada, former graduate student of Osaka University and Mr. R. Kujime, Mr. N. Arai and Mr. A. Umeda, graduate students of Osaka University, for their help for the experiments presented in this study.

The author also wish to express his thank to members of Osakada Lab. for their friendship and warm help.

Special acknowledgements are made to my wife and parents for their warm support.

This work was partially supported from the *Showahokokai* Foundation and the Research Fellowships of the Japan Society for the Promotion of Science for Young Scientists, and these supports are gratefully acknowledged.

CONTENTS

CHAPTER 1

INTRODUCTION

1.1 Mushy-State Forming

To save material and energy in manufacturing, precision forming and near net shape forming, which requires further processing, are demanded and mushy-state forming (or semi-solid forming) is one method of meeting these needs. The forming process of a solid metal heated to a temperature of partial melting is called thixoforming, and that of a liquid metal cooled down to a temperature of partial solidification is rheoforming or rheocasting. These forming methods necessitate fewer forming processes than conventional casting or hot forming, and they are expected to have the following advantages [1,2]:

(1) Since solid and liquid are mixed and the flow stress is low, high workability is possible with a small working load using small and simple equipment.
(2) Because of the high fluidity, complex shapes can be given and near net shape forming is feasible.
(3) It is possible to mass-produce long or thin products of hardly formable materials.
(4) Fine grains and a uniform distribution of precipitation can prevent internal defects and improve mechanical properties such as strength, extending the life of products.
(5) New compound materials can be manufactured homogeneously by mixing materials having different relative densities.
(6) Because of a low working load, the forming process requires less energy.

Mushy-state forming is developed by improving the methods for manufacturing and forming the metallic slurry. In the early 1970's, a manufacturing method for the metallic slurry was developed by Flemings *et al.* and research into the effect of grain shape on the fluidity of semi-solid metals were carried out. Machines for the continuous manufacturing of metallic slurry were contrived based on experiments

for solidification with rotary stirring and other methods [3,4] were developed. Mechanical properties of metallic slurry were reported [5-10] and models for analysis were proposed [11-15]. Casting, forging, rolling and extrusion in the mushy state have been developed and research in the development of materials using mushy-state forming was performed [16-22]. Some automotive components made of aluminium alloy were manufactured by mushy-state forming [23].

1.2 Analysis of Mushy-State Forming

Since the mushy-state metal has different deformation properties from both solid and liquid metals, methods for forming the metallic slurry and basic forming properties have been investigated mainly by experiments. Since only a few experiments and limited knowledge about the mushy-state metals have been recorded, it is difficult to design the forming processes and decide the optimum working conditions, and thus it is desired to use numerical simulations.

The finite element method is one of the numerical simulation methods that are used in various engineering fields, and it is also used for the numerical simulation for mushy-state forming. Łapkowski *et al.* [12] and Koç *et al.* [24] modelled a mushy-state metal as a viscoplastic material and the flow stress obtained in the experiments is used in the simulations. Toyoshima *et al.* [13] proposed a model that a mushy-state material is a porous material filled with a liquid component, and Kiuchi *et al.* [25] and Kang *et al.* [26] used the Toyoshima's model. The deformation behaviour of the mushy-state metal, however, depends on its shape, size and distribution of grains. Continuum models such as the finite element method cannot treat microscopic parameters. Consequently, the calculated deformation behaviour differs somewhat from the experimental one.

1.3 Distinct Element Method

The distinct element method [27-69] is one of the granular models [70-74] to overcome the limits of the continuum models in treating the motion of many grains in mushy-state forming or powder forming. In the distinct element method, a granular material is modelled to an assembly of particles, namely distinct elements, and each

particle is an element. In the case of contact between elements, the spring-dashpot model shown in Fig. 1.1 is considered and the interactive force is calculated. The elements are considered not to deform, and the virtual overlap between the elements is caused. The elastic repulsive force is obtained by multiplying the virtual overlap by the spring stiffness of the elements, and then the motion of the elements is calculated by solving Newton's equations of motion.

In the distinct element method, rectangular [27,30,31] and circular [28,32-43,64-67] elements are used in two-dimensional simulations. Circular elements are mainly used because the simulation using rectangular elements requires a large storage capacity for parameters of the elements such as position and shape and a long computing time for detecting contact between the elements. Since the circular element (in two-dimensional analysis) and the spherical element [29,44-47,65,66,68] (in three-dimensional analysis) cannot express phenomena that depend on the shape of real grains, elements of various shapes such as elliptical [48-59], hexagonal [60], ellipsoidal [61] and combined spherical [62,63] have been used.

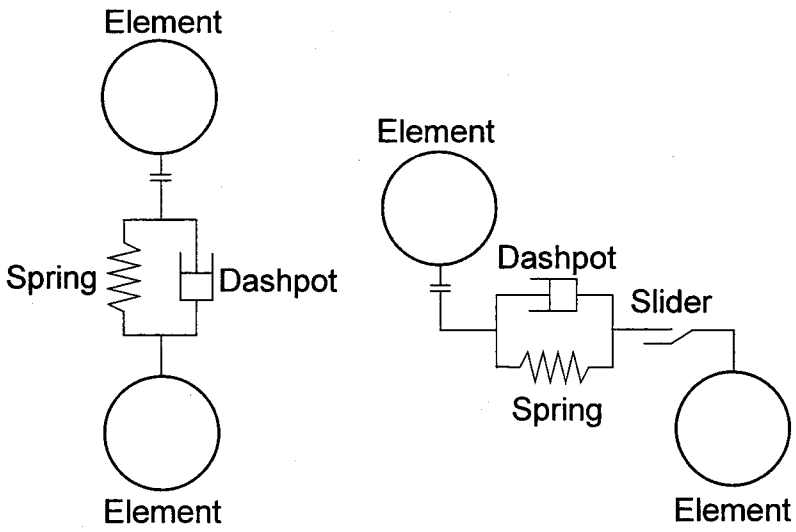

(a) Normal (b) Tangential

Fig. 1.1 Spring-dashpot model used in distinct element method.

Although the distinct element method is mainly used in soil mechanics and geotechnology, it has been applied to forming. The distinct element method is used in analyses of compaction [32,33,44-47,58,73,74], sintering [39] and extrusion [59] of metallic powders, metal injection moulding [40,41], the motion of metallic powder in a magnetic field [38,42,58] and the grain alignment of mushy-state forming [48-53,61]. Since the simple spring-dashpot model is used for calculating the force acting on the element, plastic deformation of the element is neglected. Further, forces such as the working load can be obtained qualitatively, but not quantitatively.

1.4 Research Objective

1.4.1 Grain Alignment of Mushy-State Magnet

Rare-earth magnets such as Nd-Fe-B [75] are increasingly produced recently because of their high magnetic properties. Grains have magnetic anisotropy and the magnetic properties are enhanced by aligning the direction of easy magnetisation of the grains. Rare-earth magnets are generally produced from powder metallurgy and magnet powder is formed in the magnetic field. Powder forming requires many forming processes and is not suitable for mass production. The strength of products derived from powders is low, and moreover, the attainable size of the product is small. To improve these shortcomings, a cast method of rare-earth magnets using Pr-Fe-B [76-79] has been recently developed. The as-cast magnets are worked by mushy-state forging or rolling to align the grains mechanically because the degree of grain alignment of the as-cast magnet is not high. In mushy-state forming, the boundaries of the grains melt and the rotation of the grains becomes easy. The grains cannot be aligned by magnetic forces because the magnet heated to the mushy state loses its magnetic properties. Although working conditions in the mushy-state forming of rear-earth magnets are determined in industry by trial and error experimentation, the acquired information is not enough yet. Since only limited knowledge and experience have been accumulated that would aid the design of this new process, it is desirable to develop a method for simulating the grain alignment in mushy-state forming.

The first aim of this dissertation is to establish a method for simulating the

motion of grains in mushy-state forming of magnet on the basis of the distinct element method. The individual grains of the magnet are modelled as elements in the distinct element method, and the grain alignment of the mushy-state magnet is simulated. A model experiment is carried out to examine the accuracy of the calculated results.

1.4.2 Distribution of Solid Fraction

In the beginning of mushy-state forging, only a part of the billet is in contact with the die and most of its surface is free. As the billet is compressed, the liquid component tends to flow separately from the solid component. In many such cases, the liquid component moves toward the surface layers and in some cases, furthermore, flows out of the billet during the deformation. Since the squeezed liquid component is concentrated at the surface layers, the internal structure of the forged product in the mushy state becomes heterogeneous and most of the surface layers generally consist of the structure made from the liquid component.

Although this heterogeneous distribution of the internal structure is not desirable in most cases, it may be possible to utilise the distribution for functionally gradient material. Since mushy-state metals are easy to join with other metals, more than two billets made of different kinds of metal can be joined and formed simultaneously by mushy-state forging to obtain combined products. It is required to develop the technology for controlling the flow of the liquid component, and design the billet and the forging process to obtain the desired internal structure of the product.

The second aim of this dissertation is to develop the distinct element simulation method taking into account the pressure of the liquid phase in mushy-state forming. The deformation behaviour and the distribution of the pressure of the liquid phase and solid fraction are investigated by the simulation of mushy-state upsetting.

1.5 Outline of Dissertation

It is difficult to simulate mushy-state forming by the continuum models such as the finite element method because the deformation behaviour is effected by the shape and the size of the grain. As examples of mushy-state forming, the grain alignment of

rare-earth magnet in mushy-state forging and the distribution of solid fraction in mushy-state upsetting are treated in this dissertation.

This dissertation consists of seven chapters:

Chapter 2 presents the formulation for the distinct element method using elliptical elements. In order to treat the grain alignment of rare-earth magnet in mushy-state forging, the forming process is approximated to the plane-strain deformation and the grains are modelled as an assembly of elliptical elements. The effects of reduction in height, solid fraction and grain aspect ratio on the degree of grain alignment are investigated. The distribution of the degree of grain alignment is also investigated.

In Chapter 3, the distinct element simulation presented in Chapter 2 is applied to decide the optimum working conditions in mushy-state forging of rare-earth magnet. In the optimisation of the working conditions, the degree of grain alignment and the crop loss are evaluated. The aspect ratio of the magnet, the volume rate of the capsule and the die angle are selected for optimising working conditions. The volume rate of the capsule and the die angle are fixed and the aspect ratio of the magnet is optimised, first. Next, the volume rate of the capsule is optimised using the fixed die angle and the optimised aspect ratio of the magnet. Finally, the die angle is optimised with the optimised aspect ratio of the magnet and volume rate of the capsule.

Chapter 4 presents the formulation for the three-dimensional distinct element method using ellipsoidal elements. A simulation and a model experiment of mushy-state forging of rare-earth magnet are performed. Two and three-dimensional calculated results for degree of grain alignment are compared. The distribution of the degree of grain alignment is also investigated.

In Chapter 5, the formulation for the two-dimensional distinct element method including the pressure of the liquid phase is proposed. The distribution of solid fraction in mushy-state forming is investigated. The solid particles are modelled as circular solid elements and the liquid phase is divided into triangular liquid elements having different values of pressure. The triangular liquid elements are generated by connecting the centres of the circular solid elements by means of the Delaunay triangulation.

Chapter 6 presents the formulation for the three-dimensional distinct element method including the pressure of the liquid phase. The solid particles and the liquid phase are modelled as spherical solid and tetrahedral liquid elements, respectively. The

distribution of solid fraction in mushy-state forming is studied.

Finally, the concluding remarks for the present study are given in Chapter 7.

References

[1] M. Kiuchi, Development of metal forming process in mashy-state, *J. Japan Soc. Technol. Plasticity*, **22**-247 (1981), 767-773. (In Japanese)

[2] M. Kiuchi, Characteristics and processings of metals in mashy state, *Trans. Japan Institute of Metal*, **21**-9 (1982), 687-695. (In Japanese)

[3] M.C. Flemings, Behavior of metal alloys in the semisolid state, *Metallurgical Trans. B*, **22B** (1991), 269-293.

[4] K. Ichikawa, Present status of rheocast process, *J. ISIJ*, **74**-1 (1988), 51-60. (In Japanese)

[5] M. Kiuchi, S. Fukuoka and K. Arai, Flow stress and deformation behaviors of metals (alloys) in their mashy state, *J. Japan Soc. Technol. Plasticity*, **17**-186 (1976), 595-602. (In Japanese)

[6] M. Kiuchi, S. Sugiyama and K. Arai, Flow stress and deformation behaviour of alloy in mashy state (Study of metal forming in mashy state I), *J. Japan Soc. Technol. Plasticity*, **20**-223 (1979), 762-769. (In Japanese)

[7] M. Yoshikawa, Pressure-forging of semi-solid metals and its material quality, *J. Japan Soc. Technol. Plasticity*, **22**-247 (1981), 760-766. (In Japanese)

[8] G. Shin, T. Kajitani, T. Suzuki and T. Umeda, Mechanical properties of carbon steels during solidification, *J. ISIJ*, **78**-4 (1992), 587-593. (In Japanese)

[9] M. Suery and M.C. Flemings, Effect of strain rate on deformation behaviour of semi-solid dendritic alloys, *Metallurgical Trans. A*, **13A** (1982), 1809-1819.

[10] P.O. Charreyron and M.C. Flemings, Rheology of semi-solid dendritic Sn-Pb alloys at low strain rates: Application to forming process, *Int. J. Mech. Sci.*, **27**-11/12 (1985), 781-791.

[11] L.A. Lalli, A model for deformation and segregation of solid-liquid mixtures, *Metallurgical Trans. A*, **16A** (1985), 1393-1403.

[12] W. Łapkowski, M. Pietrzyk and J. Sinczak, *J. Mater. Process. Technol.*, **34** (1992), 481-488.

[13] S. Toyoshima and Y. Takahashi, A numerical simulation of forming processes for semi-solid materials, *ISIJ Int.*, **31**-6 (1991), 577-582.

[14] M. Kiuchi, S. Fukuoka and K. Arai, Examination of extrusion process of alloys in their mashy state, *J. Japan Soc. Technol. Plasticity*, **18**-199 (1977), 633-640. (In Japanese)

[15] E. Fras, W. Kapturkiewicz and A. Burbielko, Micro-macro modeling of casting solidification controlled by transient diffusion and undercooling, *Modelling of casting, welding and advanced solidification process VII*, (The Minerals, Metals and Materials Society, M. Cross and J. Campbell ed.), (1995), 679-686.

[16] M. Kiuchi, S. Sugiyama and K. Arai, Extrusion of alloys in mashy state (Study of metal forming in mashy state II), *J. Japan Soc. Technol. Plasticity*, **20**-224 (1979), 826-833. (In Japanese)

[17] T. Matsumiya and M.C. Flemings, Modeling of continuous strip production by rheocasting, *Metallurgical Trans. B*, **12B** (1981), 17-31.

[18] M. Kiuchi and S. Sugiyama, Production of clad metals by mashy state extrusion (Experimental study on metal forming in mashy state 3rd report), *J. Japan Soc. Technol. Plasticity*, **22**-258 (1982), 700-707. (In Japanese)

[19] M. Kiuchi and S. Sugiyama, Investigation into mashy-state processing and working of particle reinforced composite metals (Experimental study on metal forming in mashy-state IV), *J. Japan Soc. Technol. Plasticity*, **23**-260 (1982), 915-923. (In Japanese)

[20] M. Kiuchi, S. Sugiyama, N. Endo and M. Kuwasaki, An investigation into mashy-state forging of particle reinforced composite metals (Experimental study of metal forming in mashy-state V), *J. Japan Soc. Technol. Plasticity*, **24**-272 (1983), 974-980. (In Japanese)

[21] M. Kiuchi, S. Sugiyama and N. Endo, Production and working of particle reinforced clad-metals by mashy-state processes (Experimental study of metal forming in mashy-state VI), *J. Japan Soc. Technol. Plasticity*, **24**-274 (1983), 1113-1119. (In Japanese)

[22] M. Kiuchi, S. Sugiyama and M. Arai, Mashy-state forging of cast-iron, *J. Japan Soc. Technol. Plasticity*, **37**-430 (1996), 1219-1224. (In Japanese)

[23] *Nikkei New Materials*, **6** (1992), 10-23. (In Japanese)

[24] M. Koç, V. Vazquez, T. Witulski and T. Altan, Application of the finite element method to predict material flow and defects in the semi-solid forging of A356 aluminum alloys, *J. Mater. Process. Technol.*, **56** (1996), 106-112.

[25] M. Kiuchi and J. Yanagimoto, Numerical simulation of deformation behaviour for semi-solid materials, *Proc. 1994 Japanese Spring Conf. Technol. Plasticity*, (1994), 447-450. (In Japanese)

[26] C.G. Kang and J.H. Yoon, A finite-element analysis on the upsetting process of semi-solid aluminum material, *J. Mater. Process. Technol.*, **66** (1997), 76-84.

[27] P.A. Cundall, A computer model for simulating progressive, large-scale movements in blocky rock systems, *Proc. Symp. Soc. Int. Rock Mech.*, Nancy **2**-8 (1971).

[28] P.A. Cundall and O.D.L. Strack, A discrete numerical model for granular assemblies, *Geotechnique*, **29** (1979), 47-65.

[29] P.A. Cundall, Computer simulations of dense sphere assemblies, *Micromechanics of granular materials*, (Elsevier Science, M. Satake and J.T. Jenkins ed.), (1988), 113-123.

[30] G.A. Kohring, S. Melin, H. Puhl, H.J. Tillemans and W. Vermöhlen, Computer simulations of critical, non-stationary granular flow through a hopper, *Comp. Meth. Appl. Mech. Eng.*, **124** (1995), 273-281.

[31] J. Ghaboussi, Fully deformable discrete element analysis using a finite element approach, *Comp. Geotech.*, **5** (1988), 175-195.

[32] S. Shima, J. Lian and K. Asada, Numerical experiments on powder characteristics and packing of powder materials, *Compaction & Consolidation Process, Adv. Powder Met. & Particulate Mat.*, **2** (1992), 85-97.

[33] S. Shima and G. Sugiyama, Simulation of behaviour of granular material by particulate modeling, *Proc. 13th Japan Congress Mater. Research*, (1993), 47-52.

[34] J. Lian and S. Shima, Powder assembly simulation by particle dynamics method, *Int. J. Numer. Meth. Eng.*, **37** (1994), 763-775.

[35] M.H. Sadd, A. Shukla and H. Mei, Computational and experimental modeling of wave propagation in granular materials, *Proc. 4th Int. Conf. Comp. Meth. Exp. Meth.*, (1989), 325-334.

[36] R.I. Borja and J.R. Wren, Micromechanics of granular media Part I: Generation of

overall constitutive equation for assemblies of circular disks, *Comp. Meth. Appl. Mech. Eng.*, **127** (1995), 13-36.

[37] J.R. Wren and R.I. Borja, Micromechanics of granular media Part II: Overall tangential moduli and localization model for periodic assemblies of circular disks, *Comp. Meth. Appl. Mech. Eng.*, **141** (1997), 221-246.

[38] H. Kotera, A. Onoyama and S. Shima, Behaviour of ferromagnetic granular in magnetic field and magnetic characteristics of compact by particle model, *J. Japan Soc. Powder and Powder Metallurgy*, **42**-5 (1995), 645-650. (In Japanese)

[39] F. Tsumori, S. Tamura, J. Kihara and T. Aizawa, Sintering analysis by granular modeling, *J. Japan Soc. Powder and Powder Metallurgy*, **42**-4 (1995), 501-506. (In Japanese)

[40] T. Iwai, T. Aizawa and J. Kihara, Granular flow simulation for metal injection molding process, *Int. J. Modern Phys. B*, 7-9 & 10 (1993), 2047-2056.

[41] T. Iwai, T. Aizawa and J. Kihara, Thermal and mechanical coupling in granular modeling for metal injection molding, *J. Mater. Process. Technol.*, **42** (1994), 175-185.

[42] S. Tamura, T. Aizawa and J. Kihara, Magnetic powder forming simulation subjected to pressing in magnetic field, *J. Mater. Process. Technol.*, **45** (1994) 353-358.

[43] S. Tamura, T. Aizawa and J. Kihara, Magnetic field powder forming analysis by granular modeling, *J. Japan Soc. Technol. Plasticity*, **36**-416 (1995), 954-959. (In Japanese)

[44] S. Shima, H. Kotera and Y. Ujie, 3-d simulation of compaction behaviour of copper powder based on particular modeling, *J. Japan Soc. Powder and Powder Metallurgy*, **42**-3 (1995), 341-346. (In Japanese)

[45] S. Shima, H. Kotera and Y. Ujie, Fundamental study of powder compaction by 3-d particulate modeling, *Proc. AEPA'96*, (Pergamon, T. Abe and T. Tsuta ed.), (1996), 159-164.

[46] S. Tamura and T. Aizawa, Mechanical behavior of powder particle on the applied vibration, *Int. J. Modern Phys. B*, 7-9 & 10 (1993), 1829-1838.

[47] S. Tamura, T. Aizawa and J. Kihara, Three-dimensional granular modeling for metallic powder compaction and flow analysis, *J. Mater. Process. Technol.*, **42**

(1994), 197-207.

[48] K. Mori, M. Otsu, K. Osakada and M. Shiomi, Simulation of grain alignment in mushy-state forging of magnets by distinct element method, *Simulation of Materials Processing: Theory, Methods and Applications*, (Balkema, S.F. Shen and P. Dawson ed.), (1995), 1185-1190.

[49] M. Otsu, K. Mori, K. Osakada and M. Shiomi, Simulation of grain alignment in plane-strain forging of mushy-state magnets by distinct element and finite element methods, *Dynamic Plasticity and Structural Behaviors The 5th International Symposium on Plasticity and Its Current Applications*, (Gordon and Breach Publishers, S. Tanimura and A.S. Khan ed.), (1995), 297-300.

[50] M. Otsu, K. Mori and K. Osakada, Simulation of grain alignment in mushy-state forming of magnets by distinct element method, *JSME series A*, **62**-594 (1996), 452-457. (In Japanese)

[51] K. Mori, M. Otsu and K. Osakada, Distinct element simulation of grain alignment in mushy-state forging of magnets, *Int. J. Mech. Sci.*, **39**-7 (1997), 771-780.

[52] M. Otsu, K. Mori and K. Osakada, Determination of optimum working conditions in mushy-state upsetting of magnet using distinct element simulation, *J. Mater. Process. Technol.*, **60** (1996), 691-696.

[53] M. Otsu, K. Mori and K. Osakada, Determination of working conditions in mushy-state forging of magnet using distinct element simulation, *JSME series A*, **63**-609 (1997), 1089-1095. (In Japanese)

[54] L. Rothenburg, Numerical simulation of idealized granular assemblies with plane elliptical particles, *Computers and Geotechnics*, **11** (1991), 315-329.

[55] L. Rothenburg and R.J. Bathurst, Effects of particle shape on micromechanical behavior of granular materials, *Advances in micromechanics of granular materials*, (Elsevier Science, H.H. Shen et al. ed.), (1992), 343-352.

[56] J.M. Ting, M. Khwaja, L.R. Meachum and J.D. Rowell, An ellipse-based discrete element model for granular materials, *Int. J. Numer. Analyt. Meth. Geomechanics*, **17** (1993), 603-623.

[57] M.A. Tzaferopoulos, On the numerical modeling of convex particle assemblies with friction, *Comp. Meth. Appl. Mech. Eng.*, **127** (1995), 371-386.

[58] H. Kotera, H. Kitahara and S. Shima, Non-circular particle behaviour under

compaction in applied magnetic fields, *J. Japan Soc. Powder and Powder Metallurgy*, **42**-9 (1995), 1019-1026. (In Japanese)

[59] H. Kotera and S. Shima, Particle dynamics simulation of powder forward extrusion, *Proc. AEPA'96*, (Pergamon, T. Abe and T. Tsuta ed.), (1996), 783-787.

[60] J. Ghaboussi and R. Barbosa, Three-dimensional discrete element method for granular materials, *Int. J. Numer. Analyt. Meth. in Geomech.*, **14** (1990), 451-472.

[61] M. Otsu, K. Mori and K. Osakada, Three-dimensional distinct element simulation of grain alignment in mushy-state forging of magnets, *Computational Plasticity Fundamentals and Applications*, (CIMNE, D.R.J. Owen, E. Oñate and E. Hinton ed.), (1997), 1387-1392.

[62] S. Yamamoto and T. Matsuoka, A method for dynamic simulation of rigid and flexible fibers in a flow field, *J. Chem. Phys.*, **98** (1993), 644-650.

[63] S. Yamamoto and T. Matsuoka, Viscosity of dilute suspensions of rodlike particles: A numerical simulation method, *J. Chem. Phys.*, **100** (1994), 3317-3324.

[64] T. Kawaguchi, T. Tanaka and Y. Tsuji, Numerical simulation of fluidized bed using the discrete element method (the case of spouting bed), *JSME series B*, **58**-551 (1992), 2119-2125. (In Japanese)

[65] T. Kawaguchi, T. Tanaka and Y. Tsuji, Numerical simulation of Two-dimensional fluidized beds using DEM (The case of spouted bed: Comparison between 2-D model and 3-D model), *JSME series B*, **61**-589 (1995), 3169-3175. (In Japanese)

[66] Y. Inoue, T. Yokoyama, K. Yamane, T. Tanaka and Y. Tsuji, DEM analysis of ball motion in a tumbling ball mill (Comparison with 2-Dimensional and 3-Dimensional calculations), *JSME series C*, **63**-606 (1997), 356-363. (In Japanese)

[67] J. Oda, M. Zang and K. Tohyama, Simulation of impact fracture behavior of laminated glass using discrete element method, *JSME series A*, **63**-607 (1997), 630-635. (In Japanese)

[68] Y. Muguruma, T. Tanaka, S. Kawatake and Y. Tsuji, Discrete particle simulation of rotary vessel mixer with baffles, *JSME series C*, **62**-601 (1996), 3335-3340. (In Japanese)

[69] T. Aizawa, Granular model for process simulation of powder forming and powder metallurgy, *J. Japan Soc. Powder and Powder Metallurgy*, **43**-10 (1996), 1159-1164. (In Japanese)

[70] S. Yuu, K. Nohara and T. Umekage, Numerical simulation of air and particle motions in 3-dimensional coarse particle turbulent fluidized bed, *JSME series B*, **62**-601 (1996), 3300-3308. (In Japanese)

[71] Y. Kishino, Investigation of the quasi-static behavior of granular materials with a new simulation method, *Proc. Japan Soc. Civil Eng.*, **406**/III-11 (1989), 97-106. (In Japanese)

[72] T. Tsuchikura, Y. Kishino and M. Satake, Granular element analysis of three-dimensional deformation mechanism of granular materials, *Proc. Japan Soc. Civil Eng.*, **436**/III-16 (1991), 111-120. (In Japanese)

[73] T. Kinoshita and S. Shima, Quasi-static simulation of powder packing behaviour by particulate modeling (1st report, two-dimensional calculation), *JSME series A*, **61**-586 (1995), 1331-1336. (In Japanese)

[74] T. Kinoshita and S. Shima, Quasi-static simulation of powder packing behaviour by particulate modeling (2nd report, three-dimensional calculation), *JSME series A*, **61**-590 (1995), 2253-2258. (In Japanese)

[75] M. Sagawa, S. Fujimura, N. Togawa, H. Yamamoto and Y. Matsuura, New material for permanent magnets on a base of Nd and Fe, *J. Appl. Phys.*, **55** (1984), 2083-2087.

[76] T. Shimoda, K. Akioka, O. Kobayashi and T. Yamagami, High-energy cast Pr-Fe-B magnets, *J. Appl. Phys.*, **64** (1988), 5290-5292.

[77] T. Shimoda, K. Akioka, O. Kobayashi, T. Yamagami, T. Ohki, M. Miyagawa and T. Yuri, Hot-working behavior of cast Pr-Fe-B Magnets, *IEEE Trans. Magnetics*, **25**-5 (1989), 4099-4104.

[78] T. Shimoda, K. Akioka, O. Kobayashi and T. Yamagami, Hot-worked anisotropic Pr-Fe-B magnets, *Proc. 10th Int. Workshop on Rare-Earth Magnets and Their Application*, (1989), 389-398.

[79] T. Shimoda, K. Akioka, O. Kobayashi, T. Yamagami and A. Arai, Current situation in development of hot-rolled R-Fe-B magnet, *Proc. 11th Int. Workshop on Rare-Earth Magnets and Their Applications*, (1990), 17-28.

CHAPTER 2

TWO-DIMENSIONAL GRAIN ALIGNMENT OF MUSHY-STATE MAGNET

2.1 Introduction

Rare-earth magnets are generally produced from powder metallurgy and sintered magnets lack strength. To improve their strength, cast rare-earth magnets have been recently developed [1-4]. The cast magnets are deformed by mushy-state forging or rolling to align the grains mechanically because grains have magnetic anisotropy. This leads to heightened magnetic properties. In mushy-state forming, the boundaries of the grains melt, thus facilitating the rotation of the grains. The grains cannot be aligned by magnetic forces because a magnet heated to the mushy state loses its magnetic properties. Since the magnetic properties are greatly influenced by the degree of grain alignment, it is important to predict the alignment induced by mushy-state forming. It is impossible, however, to simulate the motion of individual grains in mushy-state forming by continuum models such as the finite element method.

To deal with the motion of particles in granular materials, the distinct element method has been developed by Cundall [5]. In this method, a granular material is modelled by an assembly of particles, namely distinct elements, and Newton's equations of motion are solved for individual elements under interactions with neighbouring ones. Naturally, the effects of the size, shape and distribution of the particles can be taken into consideration. Although the distinct element method has been used mainly in the field of soil mechanics and geotechnology, Lian *et al.* [6] and Tamura *et al.* [7] have applied this method to powder forming processes. The distinct element method has a possibility of analysing microscopic behaviour in a deforming material.

In this chapter, a method for simulating the motion of grains in the mushy-state forming of magnets is presented on the basis of the distinct element method. The individual grains in the magnet are modelled by elliptical elements in the distinct element method.

2.2 Method of Simulation

2.2.1 Modelling of Mushy-State Forming

The cast magnets are deformed by mushy-state forming to align the grains mechanically. In mushy-state forming of magnets, the magnet is contained in a metallic capsule so as to avoid squeezing the liquid phase out, as shown in Fig. 2.1. In the present study, the distinct element method is used to simulate the motion of the grains in the magnet, and the viscoplastic finite element method is used for plastic deformation of the capsule. For the sake of simplicity, plane-strain deformation is assumed. In the distinct element method, the grains in the magnet are modelled by means of many elliptical elements [8], and the effect of the liquid component on the motion of the grains is treated as viscous resistance to the movement. The cross-sectional shape of the real grains is not circular as typically the case in the distinct element method but more closely resembles an ellipse. The distinct and the finite element simulations are separately carried out. Plastic deformation of the capsule is first calculated by the viscoplastic finite element method, and then the distinct element simulation is performed by using the calculated motion of the interface between the capsule and magnet as a boundary condition. The degree of grain alignment induced by the forming is obtained from the motions of grains. The grain alignment results from the use of elliptical elements as opposed to circular ones.

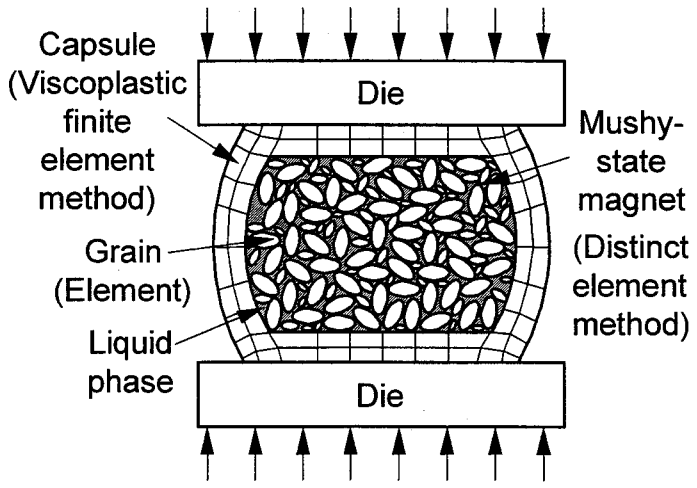

Fig. 2.1 Model for mushy-state forming of magnets using distinct and finite element methods.

2.2.2 Distinct Element Method

Since the grains in the rare-earth magnet are intermetallic compounds, the grains do not undergo plastic deformation during the forming. This is convenient to the distinct element simulation because the elements are ordinarily modelled to be rigid.

In the distinct element method, Newton's equations of motion are solved for individual elements using a small time step as follows:

$$\begin{cases} m\dot{v} + F_c + F_\ell = 0 \\ I\dot{\omega} + M_c = 0, \end{cases} \tag{2.1}$$

where m is the mass of the element, $\dot{v}$ is the acceleration, F_c is the contact force, F_ℓ is the viscous force against the liquid phase, I is the moment of inertia, $\dot{\omega}$ is the angular acceleration and M_c is the contact moment. The contact force and moment are applied to the element only in the case of the contact, whereas the viscous force invariably exists. The velocity of each element is determined by integrating the acceleration obtained from Equation (2.1) with respect to the time increment, and then the position of the element is renewed for the next step.

The contact force is composed of the elastic repulsive and frictional forces. When two elements touch as shown in Fig. 2.2, the contact force in the normal direction, F_n, by the elastic repulsion is assumed to be linear with an overlap, δ.

$$F_n = \frac{1}{2} K_n \delta , \tag{2.2}$$

where K_n is the normal spring stiffness. Since the elements are treated as being rigid, the virtual overlap, δ, between the two elements is introduced to calculate the elastic repulsive force.

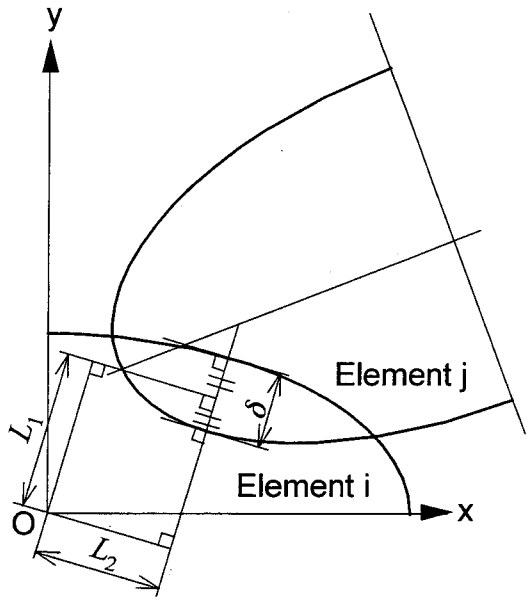

Fig. 2.2 Virtual overlap in contact of two elliptical elements.

The shape of the element is not changed even when a contact force is applied. The treatment of the contact for the elliptical elements is more complex than that for the circular ones commonly used in the distinct element method. The angle, θ (see Fig. 2.3(a)), for the normal of the ellipse passing through an arbitrary point (p,q) is expressed by

$$\alpha p \sin\theta - q\cos\theta - \left(\alpha^2 - 1\right) r \sin\theta \cos\theta = 0\,, \tag{2.3}$$

where α is the aspect ratio of the elliptical element (the ratio of the length of the major axis to that of the minor axis). The normal of element j through point A on the major axis of element i is obtained by solving Equation (2.3) by the use of the Newton-Raphson method, and point B is determined as shown in Fig. 2.3(b). The normal of element i through point B is again calculated by solving Equation (2.3). The common normal is obtained by minimising the difference of the angle, $\Delta\theta$, iteratively.

From the determined common normal, the virtual overlap between the two elements for calculating the normal contact force of Equation (2.2) is obtained. It means that the normal contact forces have the same magnitude for the two elements and are acting in the opposite directions.

The tangential contact force, F_t, induced by the elastic repulsion or the friction is expressed by

$$\begin{cases} F_t = \dfrac{1}{2} K_t \gamma & (K_t \gamma \le \mu F_n) \\ F_t = \mu F_n & (K_t \gamma > \mu F_n), \end{cases} \tag{2.4}$$

where K_t is the tangential spring stiffness, γ is relative displacement in the tangential direction calculated with the relative movement and rotation between the two elements and μ is the coefficient of friction.

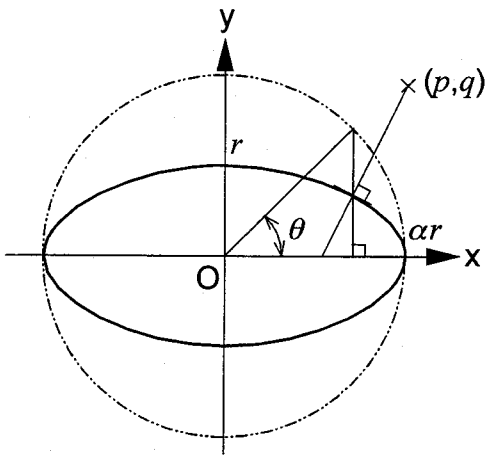

(a) Normal

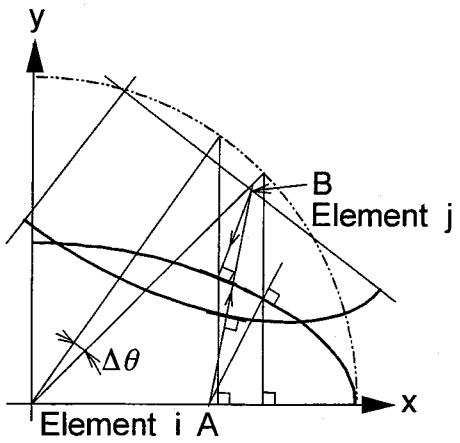

(b) Iterative calculation

Fig. 2.3 Iterative calculation of common normal to two elliptical elements.

The contact moment, M_c, is obtained from the normal and tangential contact forces using L_1 and L_2 defined in Fig. 2.2, as follows:

$$M_c = L_1 F_n + L_2 F_t . \tag{2.5}$$

From the motion of a circular cylinder in a viscous medium, the viscous force against the liquid component is approximated by

$$F_\ell = -\frac{L_3}{2\alpha r} \cdot \frac{4\pi\eta_\ell v}{\log\left(\frac{4\eta_\ell}{\alpha r \rho_\ell v}\right) - E + \frac{1}{2}}, \tag{2.6}$$

where L_3 is the projection length as shown in Fig. 2.4, η_ℓ is the coefficient of viscosity, v is the velocity, ρ_ℓ is the density of liquid and E is the Euler constant.

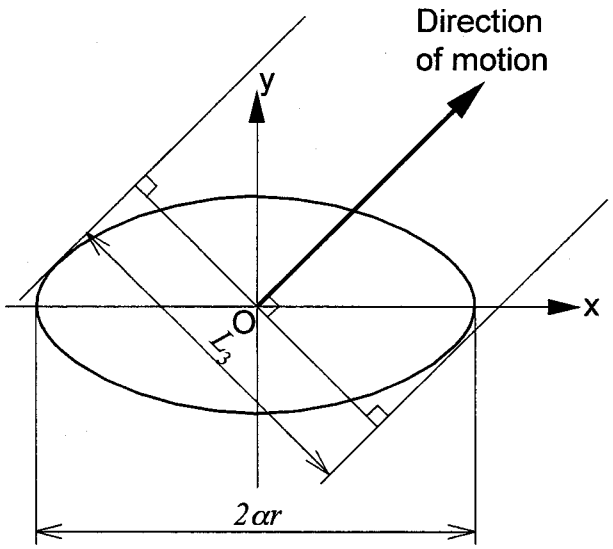

Fig. 2.4 Projection length of ellipse moving in viscous medium.

2.2.3 Viscoplastic Finite Element Method

Plastic deformation of the capsule containing the magnet is calculated by the viscoplastic finite element method. Although it is desirable that the distinct element method is coupled with the viscoplastic finite element method, the coupling is complicated. In the distinct element simulation, the pressure at the interface between the capsule and magnet is not accurately calculated because the pressure in the liquid phase is not taken into consideration. Thus, the distinct and the finite element simulations are separately carried out. Plastic deformation of the capsule is first calculated by the viscoplastic finite element method, and then the distinct element simulation is carried out by using the calculated motion of the interface between the capsule and magnet as a boundary condition.

In the viscoplastic finite element simulation, the mushy-state magnet is assumed to have a uniform distribution of the macroscopic hydrostatic pressure because the flow stress of the magnet is sufficiently smaller than that of the capsule. The volume constancy of the magnet is introduced into the viscoplastic finite element formulation by the use of the Lagrange multiplier method [9], and the following functional is minimised

$$\Phi = \int_{V_c} \left[\int_0^{\dot{\bar{\varepsilon}}} \bar{\sigma} \mathrm{d}\dot{\bar{\varepsilon}} \right] \mathrm{d}V + \int_S \tau_f \Delta v \mathrm{d}S + \lambda \dot{\varepsilon}_{vm} V_m , \tag{2.7}$$

where $\bar{\sigma}$ is the equivalent stress, $\dot{\bar{\varepsilon}}$ is the equivalent strain-rate, τ_f is the frictional shear stress, Δv is the relative velocity, λ is the Lagrange multiplier, $\dot{\varepsilon}_{vm}$ is the volumetric strain-rate of the magnet and V_c and V_m are the volumes of the capsule and magnet, respectively. The volumetric strain-rate, $\dot{\varepsilon}_{vm}$, of the magnet is expressed as a function of the nodal velocities at the interface between the capsule and magnet, and only the capsule is divided into elements. The Lagrange multiplier, λ, coincides with the macroscopic hydrostatic stress of the magnet in the minimisation. The viscoplastic finite element method for the calculation of the capsule is formulated on the basis of the plasticity theory for a material with slight compressibility [10,11]. The macroscopic information such as the working load and the deforming shape is provided by the viscoplastic finite element method.

2.3 Simulation of Mushy-State Upsetting

2.3.1 Computational Conditions

The motion of grains in mushy-state plane-strain upsetting of a rare-earth magnet contained in a mild steel capsule is simulated. The computational conditions used for the finite and the distinct element simulations are given in Table 2.1. The spring stiffness for the elastic repulsive force is obtained from the elastic finite element simulation of the plane-stain side-pressing of an elliptical bar. The relationship between the elastic repulsive force and the displacement is nearly linear.

To set the initial disposition of elements in the magnet before upsetting, the elements are first randomly located allowing overlap between elements as shown in Fig. 2.5(a), and then the distinct element simulation is continued without changing the shape of the interface between the capsule and magnet until a stable state has been reached (see Fig. 2.5(b)). By using this treatment, the initial disposition is almost random.

Table 2.1 Computational conditions used for finite and distinct element simulations of mushy-state plane-strain upsetting.

Solid fraction ψ /%	65, 70, 75, 80, 85, 87
Grain aspect ratio α	2, 2.5, 2.9
Final reduction in height $\Delta h/h$ /%	50
Number of distinct elements n	500
Coefficient of friction between distinct elements μ	0.1
Normal spring stiffness K_n /MN·mm^{-1}	65
Tangential spring stiffness K_t /MN·mm^{-1}	15
Density of solid phase /g·mm^{-3}	0.00786
Density of liquid phase ρ_ℓ /g·mm^{-3}	0.0069
Coefficient of viscosity η_ℓ /mPa·s	8
Flow stress of capsule (mild steel, 1000°C) /MPa	$\bar{\sigma} = 105\bar{\varepsilon}^{0.1}\dot{\bar{\varepsilon}}^{0.11}$
Coefficient of friction between die and capsule	0.25
Ratio of height of magnet to width	1

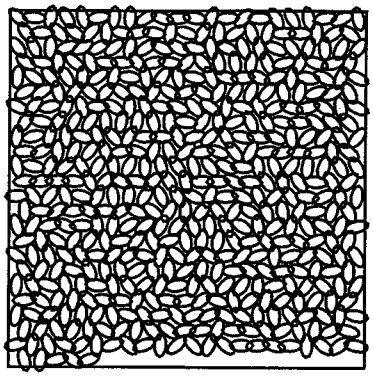

(a) Start

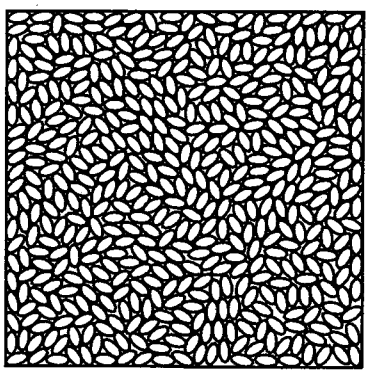

(b) Stable state

Fig. 2.5 Initial disposition of distinct elements in magnet before upsetting.

2.3.2 Model Experiment

Since real rare-earth magnets are worked at about 1000°C, model materials are used in the experiment as shown in Fig. 2.6. The mushy-state magnet is modelled by means of acrylic resin grains and a Vaseline liquid phase, and the capsule is plasticine having deformation behaviour similar to that of hot steel. The grains are produced by cutting an acrylic resin plate into elliptical discs using a laser beam. The specimen is sandwiched between two transparent acrylic resin plates to observe the motion of grains. The capsule is upset with two dies under dry friction. The cross-section of the encapsulated magnet is measured by an image scanner at every 5% reduction in height, and then the orientations of the acrylic resin grains are obtained from the measured image data using a personal computer.

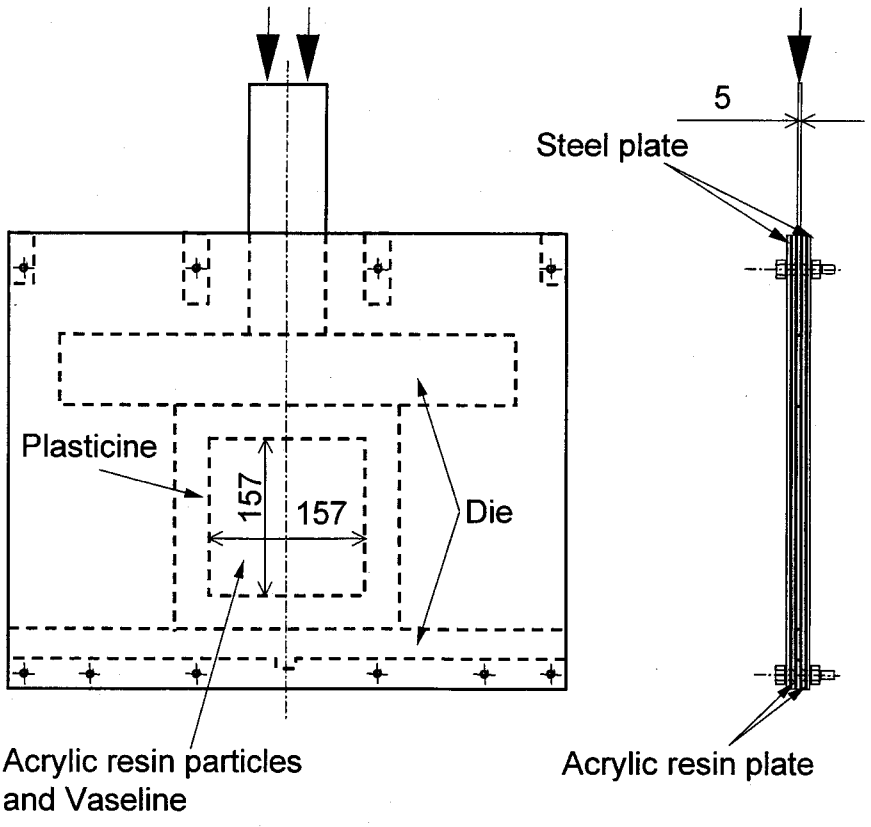

Fig. 2.6 Model experiment using acrylic resin grains and plasticine capsule.

2.3.3 Evaluation of Grain Alignment

The direction of easy magnetisation in the Pr-Fe-B rare-earth magnets is equal to that of the minor axis of the grain. By assuming that the intensity of magnetisation acts only in the direction of the minor axis, the component, H_{ui}, of the intensity of magnetisation in the upsetting direction for element i is expressed by

$$H_{ui} = H|\sin\varphi_i|, \tag{2.8}$$

where H is the intensity of magnetisation in the direction of the minor axis and φ_i is the angle of the major axis to the upsetting direction. The degree of grain alignment, A, for the magnet is defined by

$$A = \frac{1}{nH}\sum_{i=1}^{n} H_{ui}, \tag{2.9}$$

where n is the number of distinct elements. The degree of grain alignment is 1 when the minor axes of all the elements are parallel with the upsetting direction, while the degree is $2/\pi$=0.64 for the fully random orientation.

2.4 Calculated and Experimental Results

Since the calculated results depend on the initial disposition of the grains, the calculation is performed for three initial dispositions of the grains. On the other hand, the model experiments are carried out only one time in each case.

The calculated motion of grains and finite element mesh in mushy-state forging for solid fraction ψ=80% and grain aspect ratio α=2 and α=2.9 are illustrated in Fig. 2.7 and Fig. 2.8, respectively. The results obtained by the finite and distinct element simulations are simultaneously shown. The distinct elements are mechanically aligned by the interaction with neighbouring ones. The distinct elements turn perpendicular to the upsetting direction as the reduction in height increases. In the case of $\Delta h/h$=50%, the liquid phase is squeezed near the side edge of the magnet. Since the direction of easy magnetisation is that of the minor axis of the grain, thin magnets are produced by mushy-state upsetting. This is convenient for miniaturising electrical products. The tendency for α=2.9 is similar to that for α=2.

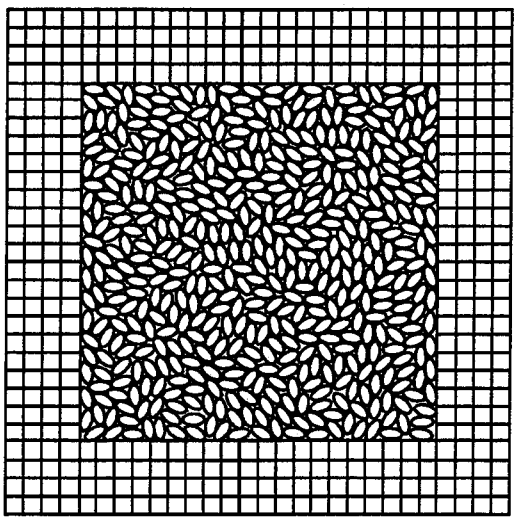

(a) $\Delta h/h$=0%

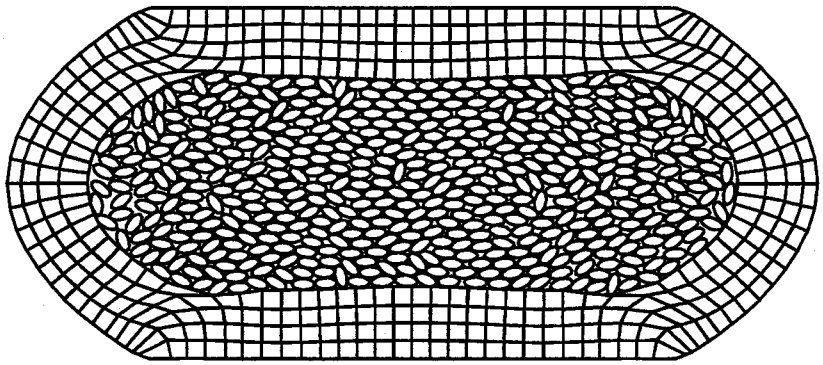

(b) $\Delta h/h$=30%

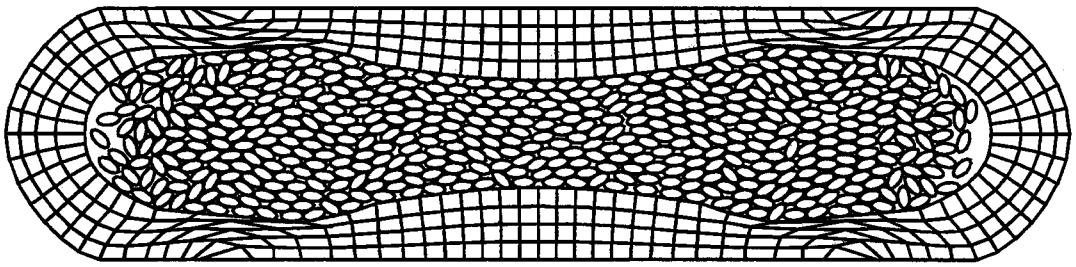

(c) $\Delta h/h$=50%

Fig. 2.7 Calculated motion of grains and finite element mesh for ψ=80% and α=2.

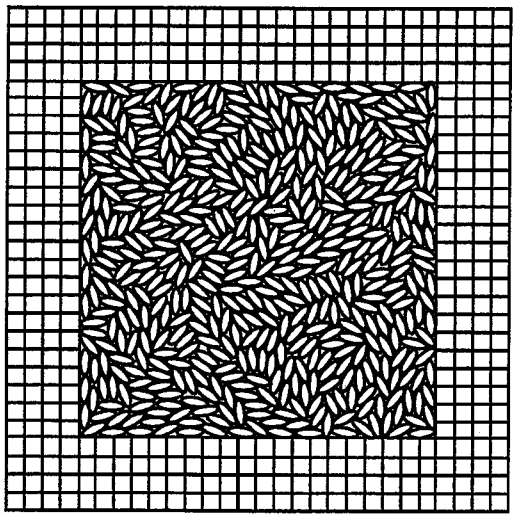

(a) $\Delta h/h$=0%

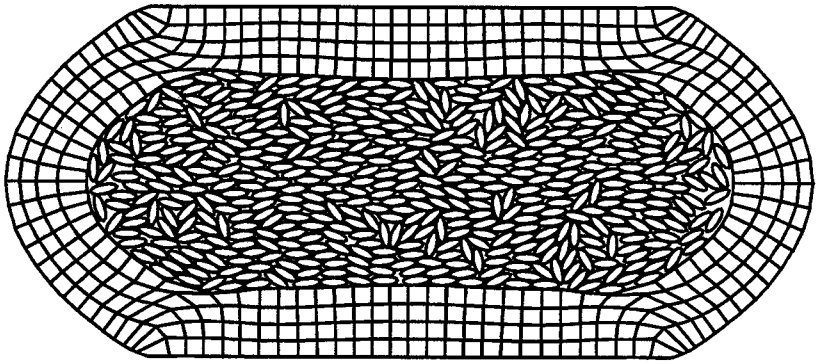

(b) $\Delta h/h$=30%

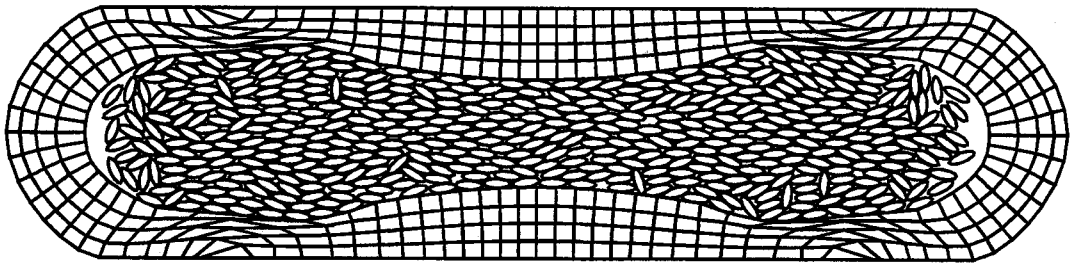

(c) $\Delta h/h$=50%

Fig. 2.8 Calculated motion of grains and finite element mesh for ψ=80% and α=2.9.

The calculated degree of grain alignment A for ψ=80% and α=2 is compared with the experimentally measured result in Fig. 2.9. Since the effect of the material properties on grain alignment is small, the properties for the rare-earth magnet and the mild steel capsule, and not the model materials, are used in the simulation. The average value for three initial dispositions is shown in this figure because the results more or less scatter for the disposition. In the initial dispositions of both calculation and experiment, the degrees of grain alignment are close to $2/\pi$=0.64, *i.e.* almost random. The degree of grain alignment increases as the height is reduced. The gradient of the grain alignment is high until the point of saturation at the height reduction of 30%. The calculated degree of grain alignment is in good agreement with the experimental result. Although the number of elements in the distinct element simulation is less than that of real magnets, the calculated tendency is similar even if the number is increased.

The distribution of the calculated degree of grain alignment for ψ=80%, α=2 and $\Delta h/h$=50% is shown in Fig. 2.10. The degree of grain alignment is large near the centre of the magnet but decreases at the sides because of insufficient compression.

The effect of the solid fraction on the degree of grain alignment for α=2, $\Delta h/h$=50% is plotted in Fig. 2.11. Although the degree of grain alignment increases with the solid fraction, the degree is almost constant in the solid fraction above 80%. This is owing to the fact that the rotation of the elements becomes difficult in the case of a high solid fraction.

The effect of the grain aspect ratio on the degree of grain alignment for ψ=80% and $\Delta h/h$=50% is illustrated in Fig. 2.12. The degree of grain alignment increases as the aspect ratio increases. When the aspect ratio exceeds 2.5 and the solid fraction is large, it is difficult to set the initial disposition of distinct elements, and the system cannot settle into a stable state.

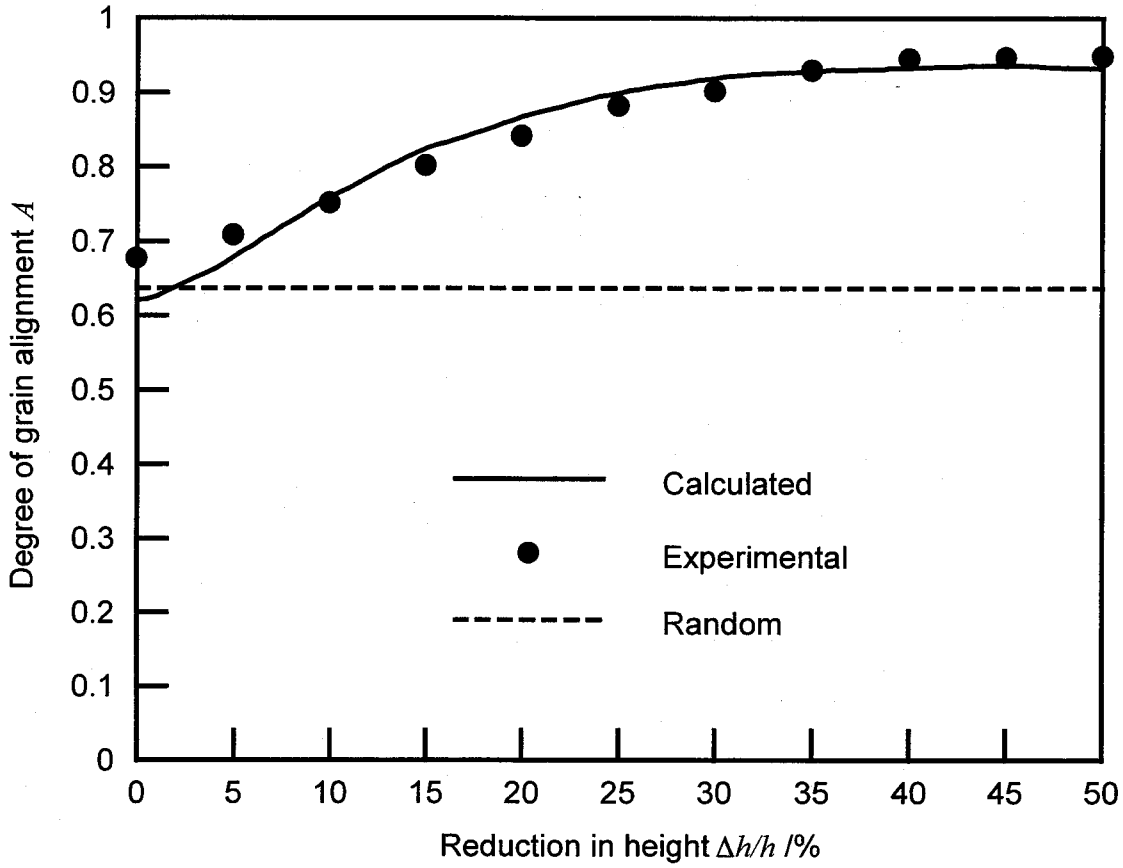

Fig. 2.9 Comparison between calculated and experimental degrees of grain alignment for ψ=80% and α=2.

0.93	0.96	0.98	0.95
0.96	0.94	0.97	0.92
0.91	0.96	0.97	0.91
0.88	0.97	0.97	0.94

Fig. 2.10 Distribution of calculated degree of grain alignment for ψ=80%, α=2 and $\Delta h/h$=50%.

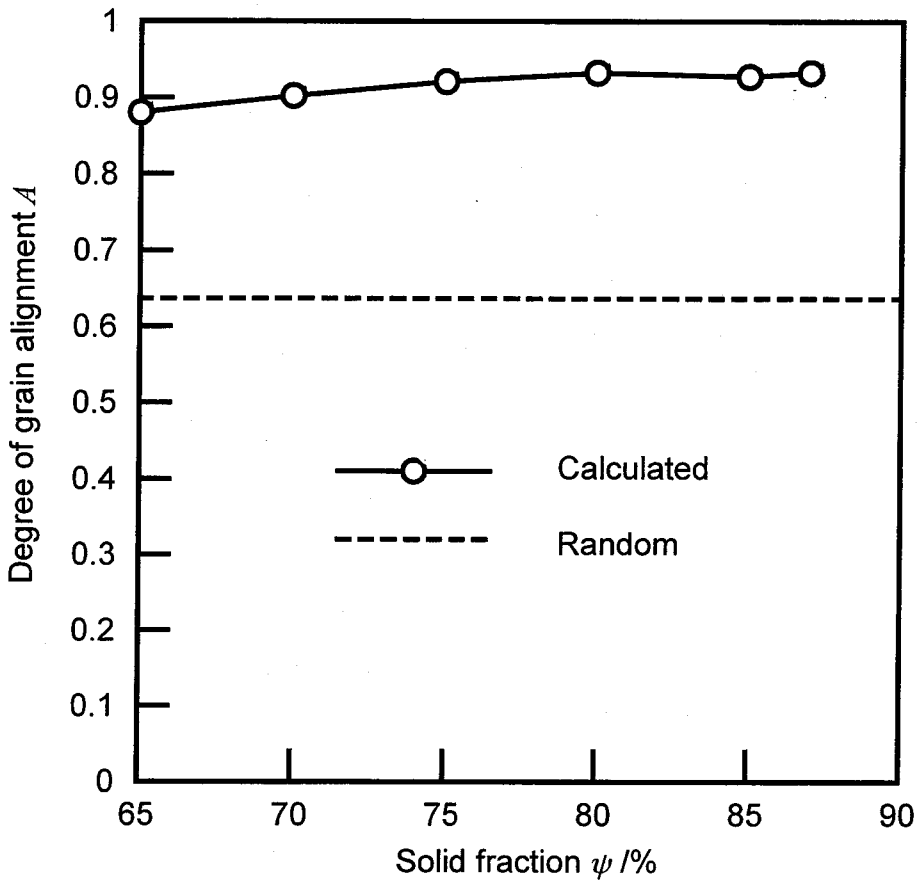

Fig. 2.11 Effect of solid fraction on degree of grain alignment for α=2 and $\Delta h/h$=50%.

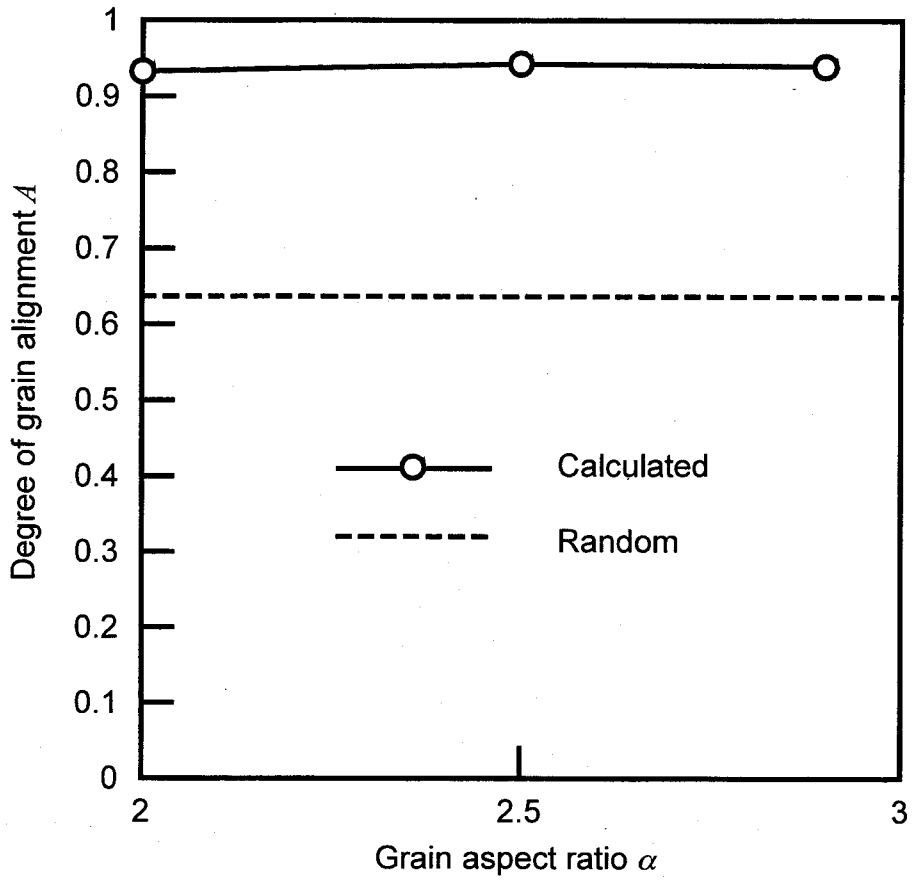

Fig. 2.12 Effect of grain aspect ratio on degree of grain alignment for ψ=80% and $\Delta h/h$=50%.

2.5 Conclusions

The motion of grains in the mushy-state forming of magnets was simulated by the distinct element method using elliptical elements. Grain alignment caused by the interaction between elements was calculated. Macroscopic plastic deformation of a metallic capsule containing the magnet was calculated by the viscoplastic finite element method, and the obtained motion of the interface between the capsule and magnet was used as a boundary condition in the distinct element simulation. Although a two-dimensional simulation was performed, the real grains of the rare-earth magnet are close to ellipsoids. It is desirable to develop a three-dimensional method using ellipsoidal elements. In the three-dimensional simulation, the treatment of the contact of ellipsoidal elements is complicated.

Although the finite element method has been widely applied to forming processes, most of these applications have been limited to the simulation of macroscopic behaviour. An extremely fine element mesh is required to simulate microscopic behaviour, and thus it takes much computing time. In this study, both microscopic and macroscopic methods were employed to compensate for each other's deficiencies. The macroscopic behaviour is first obtained by the finite element simulation, and then microscopic information is calculated from the distinct element simulation by using the obtained macroscopic information as the boundary condition. The combined approach that is proposed in this study leads to high efficiency of simulation. Such a method may have a wide range of applications in the field of forming processes.

References

[1] T. Shimoda, K. Akioka, O. Kobayashi and T. Yamagami, High-energy cast Pr-Fe-B magnets, *J. Appl. Phys.*, **64** (1988), 5290-5292.

[2] T. Shimoda, K. Akioka, O. Kobayashi, T. Yamagami, T. Ohki, M. Miyagawa and T. Yuri, Hot-working behavior of cast Pr-Fe-B Magnets, *IEEE Trans. Magnetics*, **25**-5 (1989), 4099-4104.

[3] T. Shimoda, K. Akioka, O. Kobayashi and T. Yamagami, Hot-worked anisotropic Pr-Fe-B magnets, *Proc. 10th Int. Workshop on Rare-Earth Magnets and Their Application*, (1989), 389-398.

[4] T. Shimoda, K. Akioka, O. Kobayashi, T. Yamagami and A. Arai, Current situation in development of hot-rolled R-Fe-B magnet, *Proc. 11th Int. Workshop on Rare-Earth Magnets and Their Applications*, (1990), 17-28.

[5] P.A. Cundall and O.D.L. Strack, A discrete numerical model for granular assemblies, *Geotechnique*, **29** (1979), 47-65.

[6] J. Lian and S. Shima, Powder assembly simulation by particle dynamics method, *Int. J. Numer. Meth. Eng.*, **37** (1994), 763-775.

[7] S. Tamura, T. Aizawa and J. Kihara, Three-dimensional granular modeling for metallic powder compaction and flow analysis, *J. Mater. Process. Technol.*, **42** (1994), 197-207.

[8] J.M. Ting, M. Khwaja, L.R. Meachum and J.D. Rowell, An ellipse-based discrete element model for granular materials, *Int. J. Numer. Analyt. Meth. Geomechanics*, **17** (1993), 603-623.

[9] K. Mori, K. Osakada and M. Shiomi, Finite element modelling of forming process of solid metal with liquid phase, *J. Mater. Process. Technol.*, **27** (1991), 111-118.

[10] K. Mori, K. Osakada and T. Oda, Simulation of plane-strain rolling by the rigid-plastic finite element method, *Int. J. Mech. Sci.*, **24**-9 (1982), 519-527.

[11] K. Osakada, J. Nakano and K. Mori, Finite element method for rigid-plastic analysis of metal forming-Formulation for finite deformation, *Int. J. Mech. Sci.*, **24** (1982), 459-468.

CHAPTER 3

OPTIMUM WORKING CONDITION

3.1 Introduction

Rare-earth magnets such as Nd-Fe-B [1] are increasingly produced because of their high magnetic properties. The electrical industry has a strong demand for the development of products with high magnetic properties. The magnetic properties of rare-earth magnets are enhanced by aligning the direction of easy magnetisation of the grains. This means inducing magnetic anisotropy by the forming. Although rare-earth magnets are generally produced from powder metallurgy, the strength of the products is low, and moreover the size is not large. To produce strong and large size magnets, cast rare-earth magnets using Pr-Fe-B have been recently developed [2-5]. The as-cast magnets are worked by mushy-state forging or rolling to align the grains mechanically because the degree of grain alignment of the cast magnet is not high. In mushy-state forming, the boundaries of the grains melt and the rotation of the grains becomes easy. The grains cannot be aligned by magnetic forces because the magnet heated to the mushy state loses magnetic properties. The alignment is caused by the collision between non-circular grains in the forming. It is desirable to develop a method for simulating the grain alignment in mushy-state forming because little experience and knowledge have been accumulated concerning the design of this new process.

Although the finite element method provides valuable information for the design of metal forming processes, it is impossible to simulate the motion of individual grains in the deforming metal. A method for simulating grain alignment in mushy-state forming of magnet is proposed in Chapter 2. In the proposed method, the distinct element method has been extended to the simulation of the motion of individual grains. The distinct element method is mainly used to deal with the motion of particles in granular material [6]. The proposed method is effective in determining working conditions for mushy-state forming.

In this chapter, optimum working conditions for grain alignment in mushy-state plane-strain upsetting of rare-earth magnets are obtained by the method written in chapter 2. The effects of the aspect ratio of the magnet, the volume rate of the capsule

and the die angle on grain alignment and the rate of crop loss are examined.

3.2 Evaluation and Working Conditions

3.2.1. Evaluation

The magnet exhibits an irregular shape by inhomogeneous deformation in the upsetting. Since the formed magnet is cropped into a rectangular block, it is important to reduce the crop loss from the economical point of view. Since the largest rectangle is taken from the deformed magnet as shown in Fig. 3.1, the rate of crop loss, C, is defined by

$$C = \frac{(V - V_a)}{V}, \tag{3.1}$$

where V and V_a are the volumes of the magnet before and after the cropping.

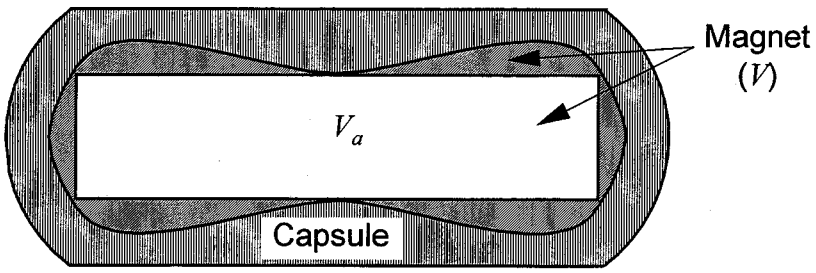

Fig. 3.1 Definition of rate of crop loss of deformed magnet.

The direction of easy magnetisation in the Pr-Fe-B rare-earth magnets is equal to that of the minor axis of the grain. By assuming that the intensity of magnetisation acts only in the direction of the minor axis, the component, H_{ui}, of the intensity of magnetisation in the upsetting direction for element i is expressed by

$$H_{ui} = H|\sin\varphi_i|, \tag{3.2}$$

where H is the intensity of magnetisation in the direction of the minor axis and φ_i is the angle of the major axis to the upsetting direction. For the cropped product, the degree of grain alignment, A, for the magnet is defined by

$$A = \frac{1}{nH}\sum_{i=1}^{n} H_{ui}, \tag{3.3}$$

where n is the number of distinct elements in the rectangular magnet after the cropping. The degree of grain alignment is 1 when the minor axes of all the elements are parallel with the upsetting direction, while the degree is $2/\pi$=0.64 for the fully random orientation.

Since the calculated results depend on the initial disposition of the grains, the calculation is performed for five initial dispositions of the grains. The degree of grain alignment is indicated as the average of five results. On the other hand, the model experiments are carried out only one time in each case.

3.2.2. Working Conditions

Mushy-state plane-strain upsetting of a rare-earth magnet contained in a mild steel capsule with concave or convex dies is investigated in the present study. The effects of the aspect ratio of the magnet, the volume rate of the capsule and the die angle on grain alignment and the rate of crop loss are examined. The aspect ratio of the magnet, ξ, is defined by

$$\xi = \frac{h_m}{w_m}, \tag{3.4}$$

where h_m and w_m are the height and width of the initial magnet part, respectively (see Fig. 3.2).

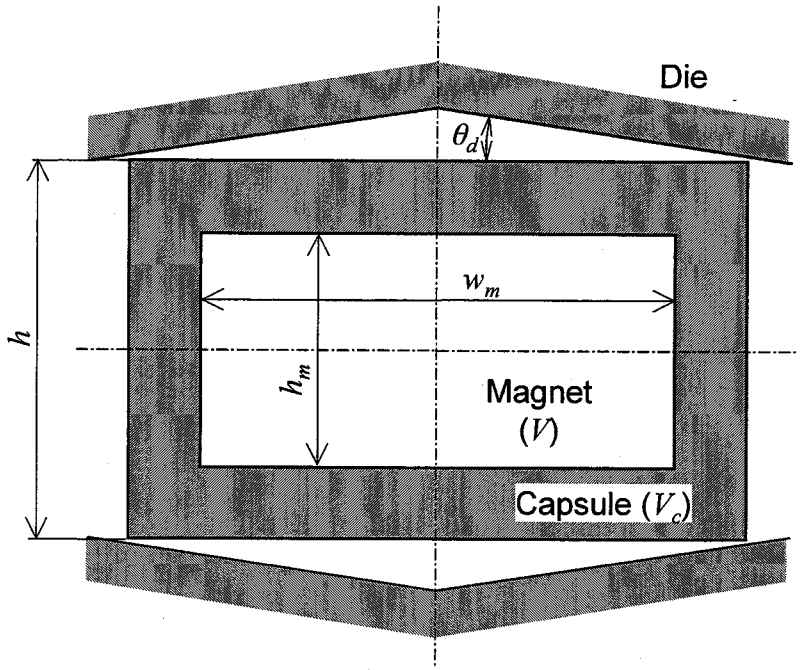

Fig. 3.2 Definition of aspect ratio of magnet and die angle.

Since the capsule is scrapped after the forming, the volume rate of the capsule, ζ, is defined by

$$\zeta = \frac{V_c}{V + V_c}, \tag{3.5}$$

where V and V_c are the volumes of the magnet and capsule, respectively.

In the optimisation of working conditions, the effect of the aspect ratio of the magnet is obtained for the volume rate of the capsule ζ=50% and the die angle θ_d=0°, and then the volume rate of the capsule is determined for the obtained aspect ratio and θ_d=0°. The die angle is finally determined for the obtained aspect ratio and volume rate. The working conditions in mushy-state upsetting and the computational conditions used for the distinct and finite element simulations are shown in Tables 3.1 and 3.2, respectively.

Table 3.1 Working conditions in mushy-state upsetting.

Aspect ratio of magnet ξ	0.33, 0.5, 0.67, 1.0, 1.5, 2.0, 3.0
Volume rate of capsule ζ /%	20, 30, 40, 50, 60
Die angle θ_d /°	-2, -1, 0, 1, 2, 3, 4, 5

Table 3.2 Computational conditions used for finite and distinct element simulations of mushy-state plane-strain upsetting.

Solid fraction ψ /%	80
Grain aspect ratio α	2
Final reduction in height $\Delta h/h$ /%	35
Number of distinct elements n	500
Coefficient of friction between distinct elements μ	0.1
Normal spring stiffness K_n /MN·mm^{-1}	65
Tangential spring stiffness K_t /MN·mm^{-1}	15
Density of solid phase /g·mm^{-3}	0.00786
Density of liquid phase ρ_ℓ /g·mm^{-3}	0.0069
Coefficient of viscosity η_ℓ /mPa·s	8
Flow stress of capsule (mild steel, 1000°C) /MPa	$\bar{\sigma} = 105\bar{\varepsilon}^{0.1}\dot{\bar{\varepsilon}}^{0.11}$
Coefficient of friction between die and capsule	0.25

3.3 Determination of Working Conditions

3.3.1. Reduction in Height

The calculated motion of grains and finite element mesh in mushy-state upsetting for the aspect ratio of the magnet ξ=0.67, the volume rate of the capsule ζ=50% and the die angle θ_d=0° are illustrated in Fig. 3.3, where $\Delta h/h$ is the reduction in height. The results obtained by the finite and distinct element simulations are simultaneously shown. The die angle θ_d is expressed as the angle between the horizontal direction and the die surface, *i.e.* concave dies for a positive value and convex dies for a negative value. The distinct elements are mechanically aligned by their interaction with neighbouring ones. The distinct elements are turned perpendicular to the upsetting direction as the reduction in height increases.

A comparison between the calculated and experimental deformed shapes of the capsule for ξ=0.67, ζ=30%, θ_d=0° and $\Delta h/h$=35% is shown in Fig. 3.4. Since the Vaseline is squeezed out from the plasticine capsule due to the high pressure, the experimental shape of the capsule after deformation is smaller than the calculated one. The magnet contained in the capsule exhibits an irregular shape, and the magnet is cropped into a rectangular shape after forming.

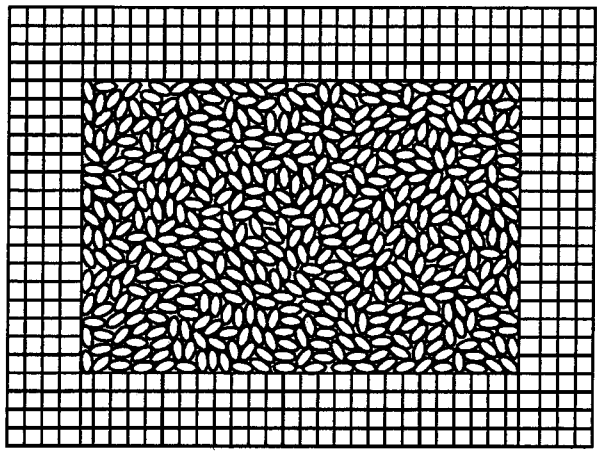

(a) $\Delta h/h$=0%

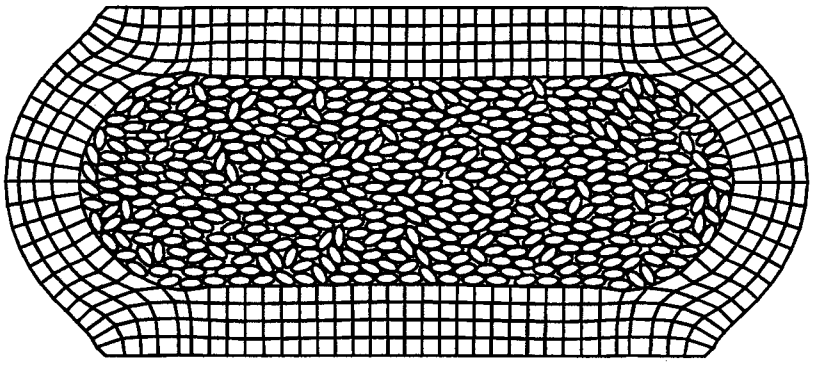

(b) $\Delta h/h$=20%

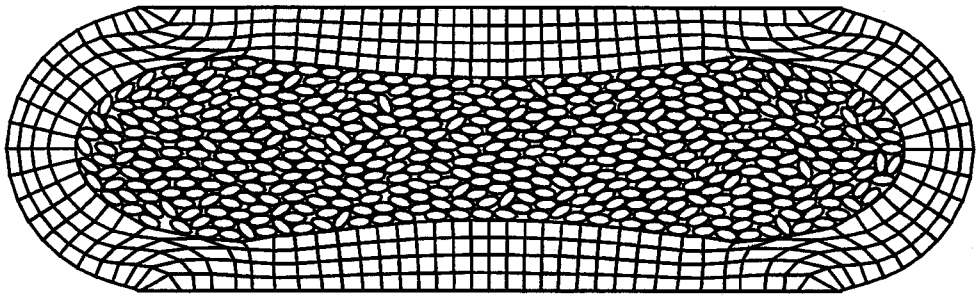

(b) $\Delta h/h$=35%

Fig. 3.3 Calculated motion of grains and finite element mesh in mushy-state upsetting for ξ=0.67, ζ=50% and θ_d=0°.

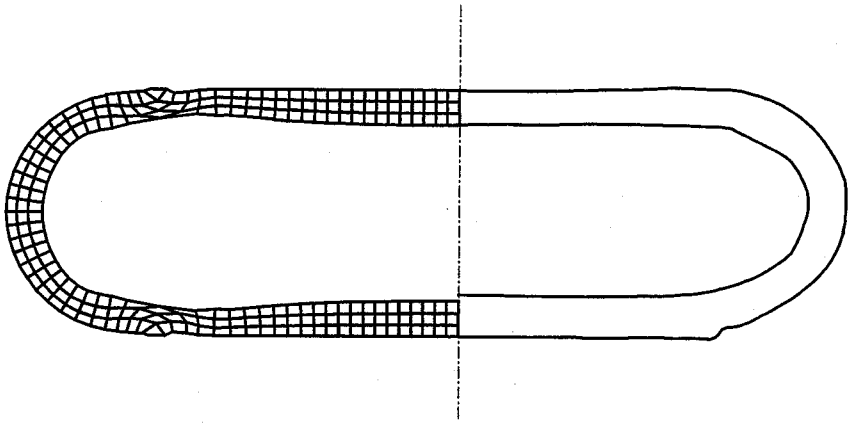

(a) Calculated (b) Experimental

Fig. 3.4 Comparison between calculated and experimental deformed shapes of capsule for ξ=0.67, ζ=30%, θ_d=0° and $\Delta h/h$=35%.

The calculated variation in the rate of crop loss C with the reduction in height for ξ=0.67 is compared with the experimentally measured one in Fig. 3.5. As the reduction in height increases, the rate of crop loss also increases.

The calculated variation in the degree of grain alignment A with the reduction in height for ξ=0.67 is compared with the experimentally measured one in Fig. 3.6. As the height is reduced, the degree of grain alignment increases. The change in the degree is relatively large, up to a 30% reduction, and then the system is saturated. The degree of grain alignment agrees well with the experimental one. Although the number of elements in the distinct element simulation is as much as that for real magnets, the calculated tendency is similar even if the number is increased.

The degree of grain alignment increases with the reduction in height, while the rate of crop loss also increases. Since the increase in the degree of grain alignment is saturated at about a 35% reduction in height, the working condition is evaluated for the 35% reduction. However, in the experiment, the volume of the magnet decreases due to the squeeze of the Vaseline, thus, the experimental result has an error. Therefore, the effects of working conditions on grain alignment are determined from the calculation.

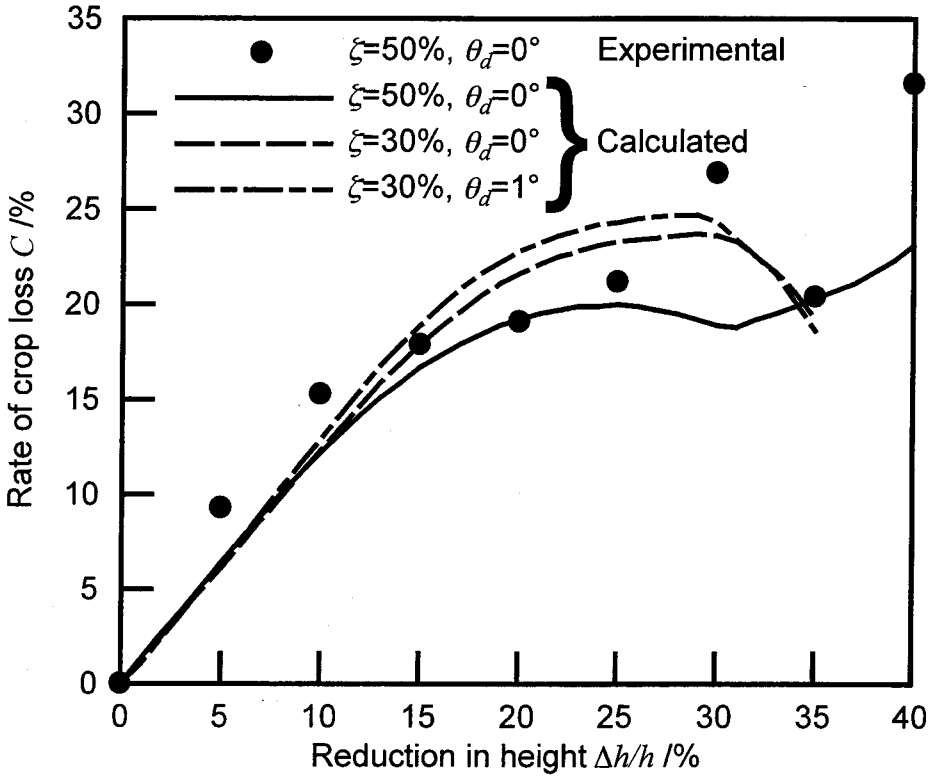

Fig. 3.5 Variation in rate of crop loss C with reduction in height for ξ=0.67.

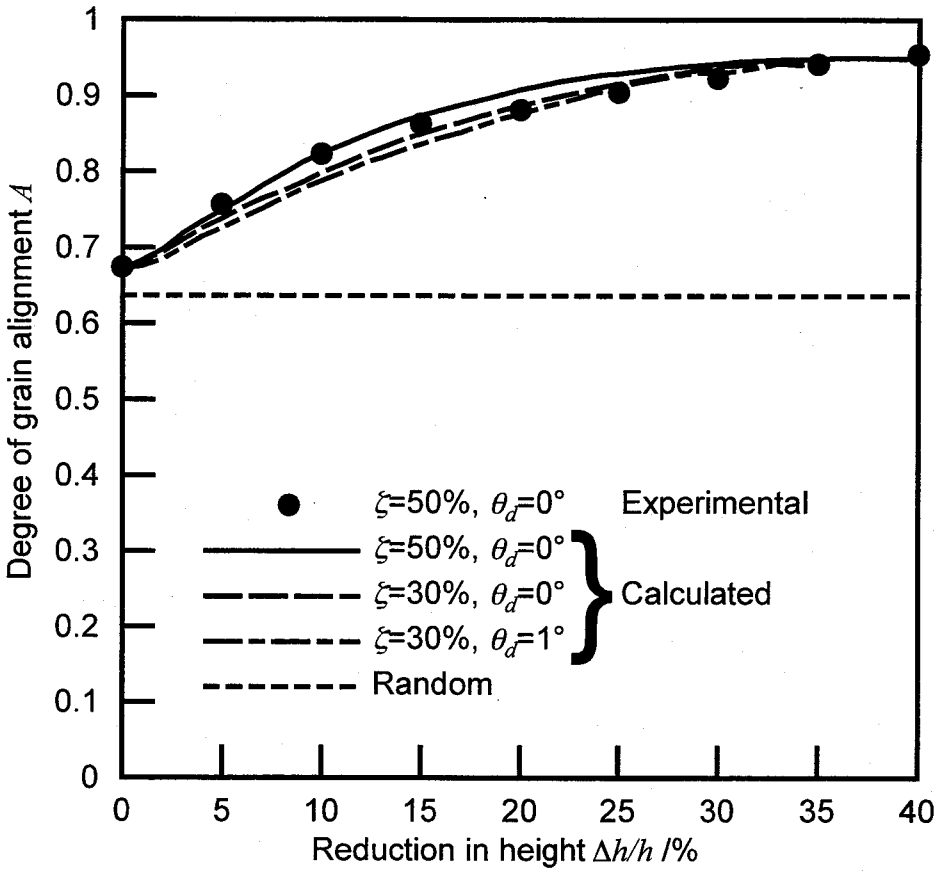

Fig. 3.6 Variation in degree of grain alignment A with reduction in height for ξ=0.67.

3.3.2. Aspect Ratio of Magnet

The effect of the aspect ratio of the magnet on the rate of crop loss for ζ=50%, θ_d=0° and $\Delta h/h$=35% is shown in Fig. 3.7. The rate of crop loss has a minimum value at ξ=0.67.

The effect of the aspect ratio of the magnet on the degree of grain alignment for ζ=50%, θ_d=0° and $\Delta h/h$=35% is illustrated in Fig. 3.8. Although the degree of grain alignment has a peak at ξ=1.0, the degree of grain alignment at ξ=0.67 and ξ=1.0 is almost the same. Since the rate of crop loss is about 20% at ξ=0.67 and about 25% at ξ=1.0, ξ=0.67 is chosen as the optimum aspect ratio of the magnet.

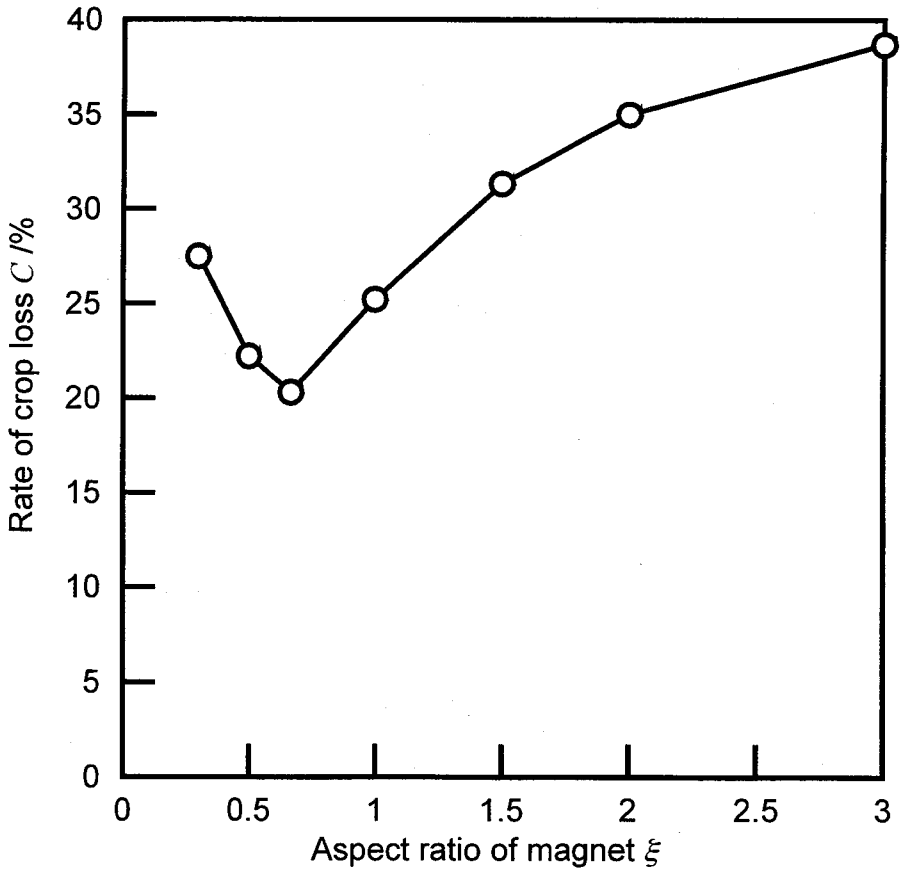

Fig. 3.7 Effect of aspect ratio of magnet on rate of crop loss for ζ=50%, θ_d=0° and $\Delta h/h$=35%.

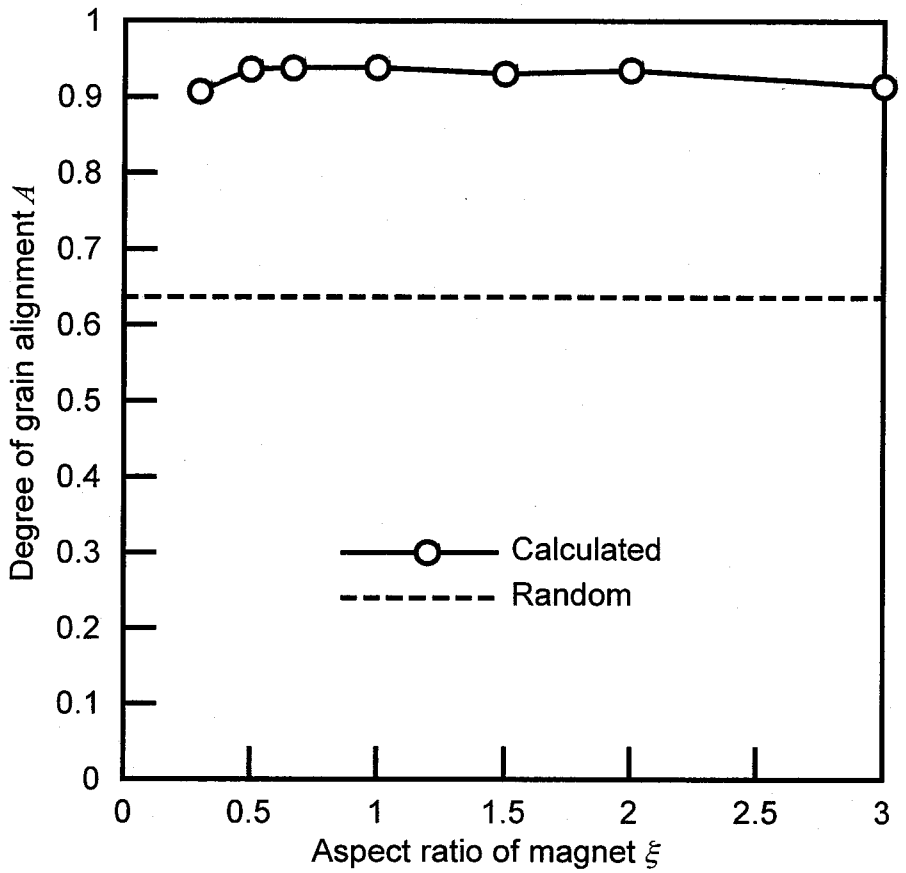

Fig. 3.8 Effect of aspect ratio of magnet on degree of grain alignment for ξ=50%, θ_d=0° and $\Delta h/h$=35%.

3.3.3. Volume Rate of Capsule

The effect of the volume rate of the capsule on the rate of crop loss for ξ=0.67, θ_d=0° and $\Delta h/h$=35% is shown in Fig. 3.9. The rate of crop loss has a minimum value at ζ=30%.

The effect of the volume rate of the capsule on the degree of grain alignment for ξ=0.67, θ_d=0° and $\Delta h/h$=35% is illustrated in Fig. 3.10. The degree of grain alignment has a peak at ζ=40%. Since the difference of the degree of grain alignment between ζ=30% and 40% is small, ζ=30% is chosen as the optimum volume rate of the capsule.

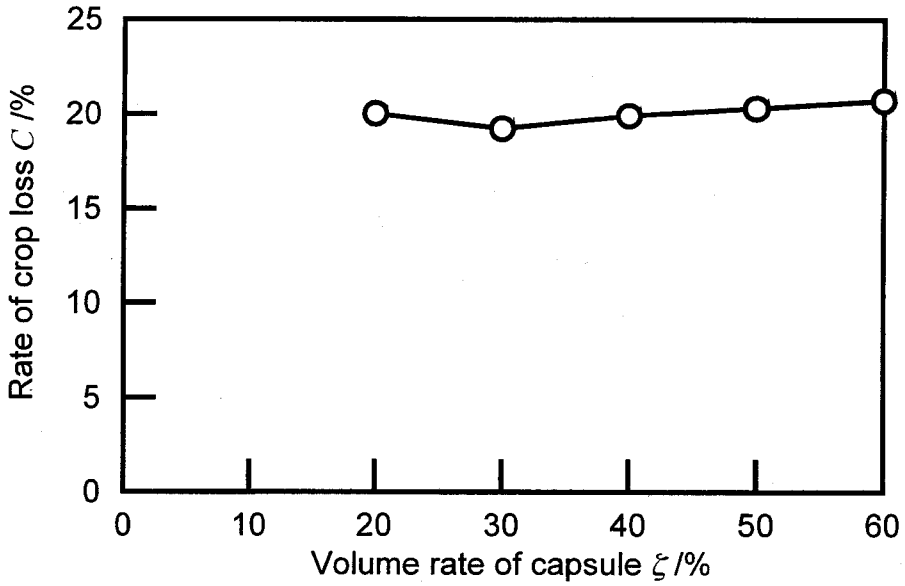

Fig. 3.9 Effect of volume rate of capsule on rate of crop loss for ξ=0.67, θ_d=0° and $\Delta h/h$=35%.

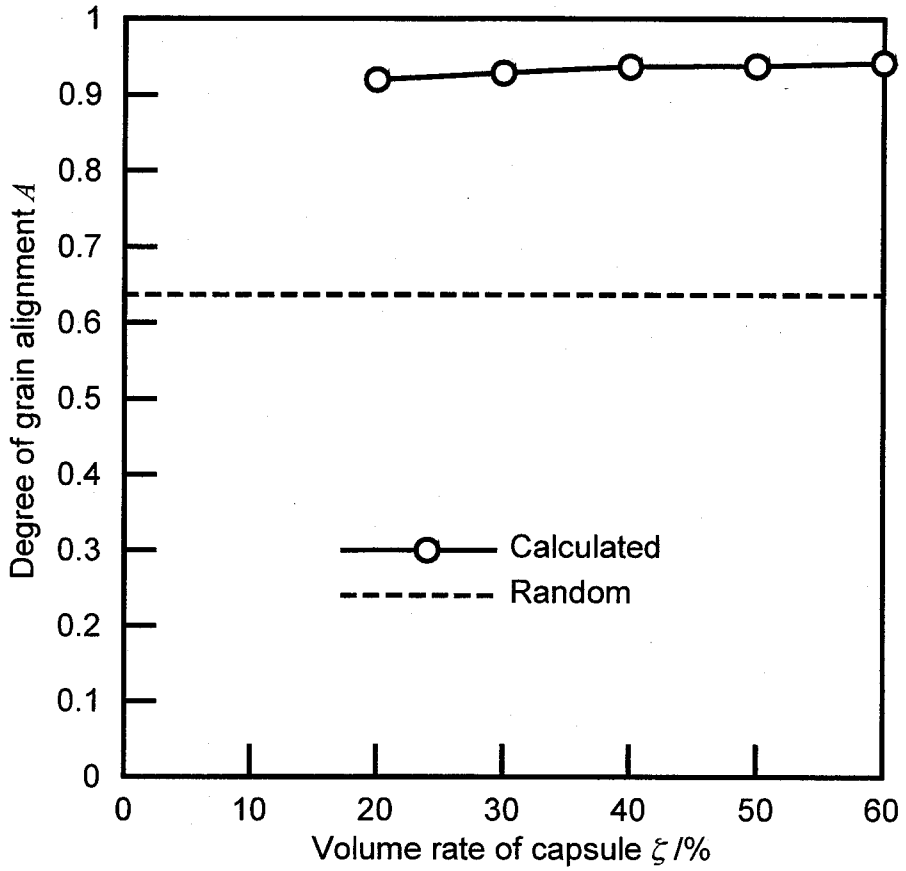

Fig. 3.10 Effect of volume rate of capsule on degree of grain alignment for ξ=0.67, $\theta_{\bar{d}}$=0° and $\Delta h/h$=35%.

3.3.4. Die Angle

The effect of the die angle on the rate of crop loss for ξ=0.67, ζ=30% and $\Delta h/h$=35% is shown in Fig. 3.11. The rate of crop loss has a minimum value at θ_d=1°.

The effect of the die angle on the degree of grain alignment for ξ=0.67, ζ=30% and $\Delta h/h$=35% is illustrated in Fig. 3.12. Since the degree of grain alignment is almost constant for the die angle, θ_d=1° is chosen.

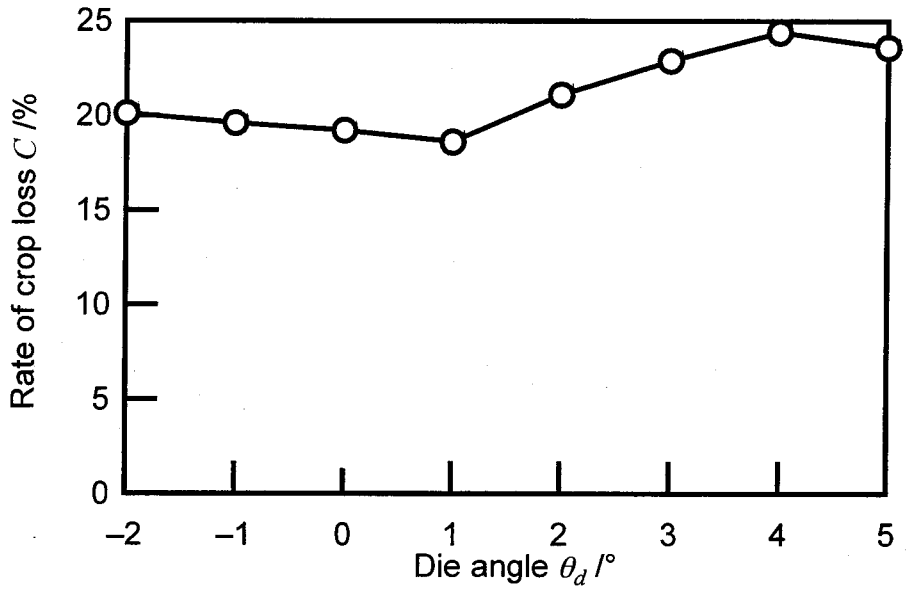

Fig. 3.11 Effect of die angle on rate of crop loss for ξ=0.67, ζ=30% and $\Delta h/h$=35%.

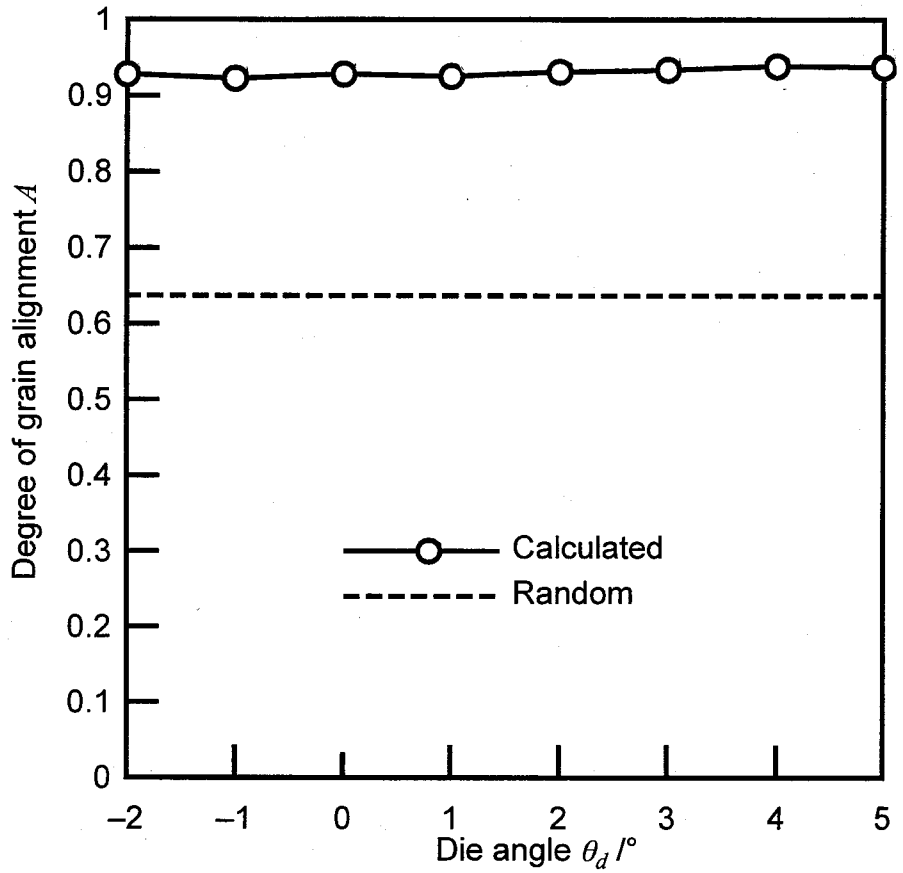

Fig. 3.12 Effect of die angle on degree of grain alignment for ξ=0.67, ζ=30% and $\Delta h/h$=35%.

3.4 Conclusions

Although working conditions in mushy-state forming of rare-earth magnets are determined in industry by trial and error experimentation, the acquired information is not enough yet. The numerical simulation using the distinct and finite element methods provides valuable information for the design of the new process. The effects of the aspect ratio of the magnet, the volume rate of the capsule and the die angle on the grain alignment and the rate of crop loss were derived from the numerical simulation. Although the effect of the reduction in height on the degree of grain alignment is large, 35% reduction is enough because of saturation. The effect of the aspect ratio of the magnet on grain alignment and rate of crop loss is comparatively large, whereas those of the volume rate of the capsule and the die angle are small.

References

[1] M. Sagawa, S. Fujimura, N. Togawa, H. Yamamoto and Y. Matsuura, New material for permanent magnets on a base of Nd and Fe, *J. Appl. Phys.*, **55** (1984), 2083-2087.

[2] T. Shimoda, K. Akioka, O. Kobayashi and T. Yamagami, High-energy cast Pr-Fe-B magnets, *J. Appl. Phys.*, **64** (1988), 5290-5292.

[3] T. Shimoda, K. Akioka, O. Kobayashi, T. Yamagami, T. Ohki, M. Miyagawa and T. Yuri, Hot-working behavior of cast Pr-Fe-B Magnets, *IEEE Trans. Magnetics*, **25**-5 (1989), 4099-4104.

[4] T. Shimoda, K. Akioka, O. Kobayashi and T. Yamagami, Hot-worked anisotropic Pr-Fe-B magnets, *Proc. 10th Int. Workshop on Rare-Earth Magnets and Their Application*, (1989), 389-398.

[5] T. Shimoda, K. Akioka, O. Kobayashi, T. Yamagami and A. Arai, Current situation in development of hot-rolled R-Fe-B magnet, *Proc. 11th Int. Workshop on Rare-Earth Magnets and Their Applications*, (1990), 17-28.

[6] P.A. Cundall and O.D.L. Strack, A discrete numerical model for granular assemblies, *Geotechnique*, **29** (1979), 47-65.

[7] K. Osakada, J. Nakano and K. Mori, Finite element method for rigid-plastic analysis of metal forming - Formulation for finite deformation, *Int. J. Mech. Sci.*, **24** (1982), 459-468.

[8] K. Mori, K. Osakada and T. Oda, Simulation of plane-strain rolling by the rigid-plastic finite element method, *Int. J. Mech. Sci.*, **24**-9 (1982), 519-527.

CHAPTER 4

THREE-DIMENSIONAL GRAIN ALIGNMENT OF MUSHY-STATE MAGNET

4.1 Introduction

Rare-earth magnets are increasingly produced because of their high magnetic properties. To improve the low strength and productivity of the magnets produced from powder metallurgy, cast rare-earth magnets using Pr-Fe-B have been recently developed [1-4]. Since the degree of grain alignment of as-cast magnets is not high enough, the as-cast magnets heated to a mushy state are worked by a forging or rolling operation to align the grains mechanically. A two-dimensional method for simulating the grain alignment in the mushy-state forming of magnets using the distinct element method is proposed in Chapter 2. The distinct element method has the capability of simulating the motion of individual grains. Since the behaviour of grains calculated by the two-dimensional method is more or less different from that for the actual forming process, *e.g.* the packing state of real grains, it is desirable to develop a three-dimensional method for simulating the grain alignment in the mushy-state forming of magnets.

The distinct element method has been developed by Cundall [5,6] to simulate the motion of particles in granular materials. In the distinct element method, the granular material is modelled as an assembly of elements representing particles, and the equations of motion for the elements are solved for small time steps. The alignment of grains in the mushy-state forming of magnets can be induced because of their non-spherical shape. For the two-dimensional simulation, rectangular [5] and elliptical [7-12] elements have been presented as non-circular elements. However, spherical elements have been used in most of three-dimensional distinct element simulations [13]. Although elements lining spheres up [14] and hexahedral elements [15] have been developed as non-spherical elements, these elements are not accurate enough for the modelling of real grains. Since the shapes of grains are similar to ellipsoids, it is realistic to develop ellipsoidal elements for the simulation of mushy-state forming.

In this chapter, a three-dimensional distinct element method using ellipsoidal elements is proposed. A scheme for treating three-dimensional contact between ellipsoidal elements is presented. The proposed method is applied to simulation of the

grain alignment in mushy-state axi-symmetric upsetting of a rare-earth magnet.

4.2 Three-Dimensional Method

4.2.1 Equation of Motion

To simulate the three-dimensional behaviour of grains in the mushy-state forming of a rare-earth magnet, a distinct element method using ellipsoidal elements is presented. Since the shape of the element is not spherical, the treatment of contact between elements and the equilibrium equations of the forces and the moment become complicated. To avoid the complexity of this formulation, the physical quantities such as the position, velocity, acceleration, force and moment are represented in vector forms. Newton's equations of motion are solved for individual elements using a small time step as follows:

$$\begin{cases} m\dot{\boldsymbol{v}} + \boldsymbol{F}_c + \boldsymbol{F}_\ell = \boldsymbol{0} \\ \boldsymbol{I} \times \dot{\boldsymbol{\omega}} + \boldsymbol{M}_c = \boldsymbol{0}, \end{cases} \tag{4.1}$$

where m is the mass of the element, $\dot{\boldsymbol{v}}$ is the acceleration, $\boldsymbol{F}_c$ is the contact force, $\boldsymbol{F}_\ell$ is the viscous force against the liquid phase, $\boldsymbol{I}$ is the moment of inertia, $\dot{\boldsymbol{\omega}}$ is the angular acceleration and $\boldsymbol{M}_c$ is the contact moment.

4.2.2 Detection of Contact

When two elements touch, a contact force is applied to these elements. Although the contact between the spherical elements is evaluated from the distance between the centres of two elements, it is not easy to treat the contact for the ellipsoidal elements. To facilitate it, a local coordinate system is introduced for each element. The origin of the local coordinate system is defined as the centre of the ellipsoid, and the z-axis coincides with the major axis of the ellipsoid.

When the ellipsoidal element touches the boundary plane as shown in Fig. 4.1, the boundary plane is expressed in the local coordinate system of the element by

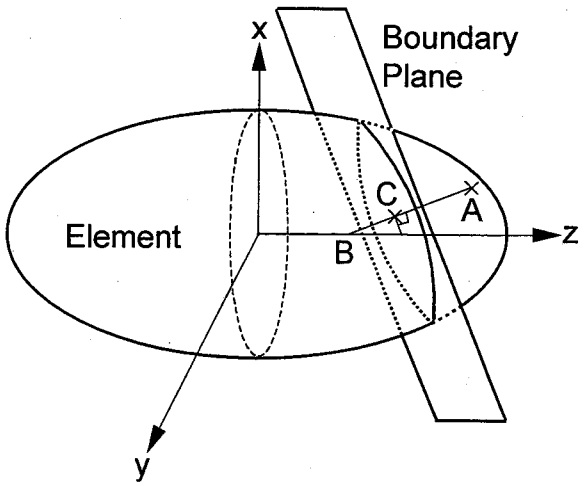

Fig. 4.1 Contact between ellipsoidal element and boundary plane.

$$ax + by + cz + d = 0, \tag{4.2}$$

where a, b, c and d are constants in the local coordinate system. The minor and major axes of the ellipsoidal element are $2r$ and $2\alpha r$ ($1<\alpha$), respectively. The common normal to the element and boundary plane is used to evaluate the contact. Points A, B and C are defined as the intersections of the common normal with the element surface, the major axis of the element and the boundary plane, respectively. The positions of points A, B and C are analytically determined as follows:

$$\left(A_x, A_y, A_z\right) = \left(\frac{a}{k}, \frac{b}{k}, \frac{\alpha^2 c}{k}\right) \tag{4.3}$$

$$\left(B_x, B_y, B_z\right) = \left(0, 0, \frac{\left(\alpha^2 - 1\right)c}{k}\right) \tag{4.4}$$

$$\left(C_x, C_y, C_z\right) = \left(at, bt, ct + B_z\right), \tag{4.5}$$

where

$$k = \frac{-d/c}{\left|-d/c\right|} \cdot \frac{\sqrt{a^2 + b^2 + \left(\alpha c\right)^2}}{r} \tag{4.6}$$

$$t = -\frac{\left(cB_z + d\right)}{a^2 + b^2 + c^2}. \tag{4.7}$$

The overlap, δ, between the ellipsoidal element and the boundary plane is presented by

$$\delta = \overline{BA} - \overline{BC}. \tag{4.8}$$

When the value of δ is positive, the element is in contact with the boundary plane.

For the contact between two ellipsoidal elements, a common normal to the elements is searched as shown in Fig. 4.2. Points A and B are defined as the intersections of the common normal with the surface and the major axis of the elements, respectively. Points A and B are given in the local coordinate system (see Fig. 4.3) by

$$(A_x, A_y, A_z) = (r\sin\theta\cos\phi, r\sin\theta\sin\phi, \alpha r\cos\theta) \tag{4.9}$$

$$(B_x, B_y, B_z) = \left(0,0,\left\{\alpha - \frac{1}{\alpha}\right\} r\cos\theta\right). \tag{4.10}$$

The equation of a normal of an ellipsoidal element through point $P(P_x, P_y, P_z)$ is expressed as follows:

$$\alpha P_z \cos\phi\sin\theta - \sqrt{P_x^2 + P_y^2}\cos\theta - (\alpha^2 - 1) r\cos\phi\sin\theta\cos\theta = 0, \tag{4.11}$$

where

$$\cos\theta = |\cos\theta^*| \frac{|P_x|}{P_x} \tag{4.12}$$

$$\sin\theta = |\sin\theta^*| \frac{|P_y|}{P_y} \tag{4.13}$$

$$\theta^* = \tan^{-1}\frac{P_y}{P_x}. \tag{4.14}$$

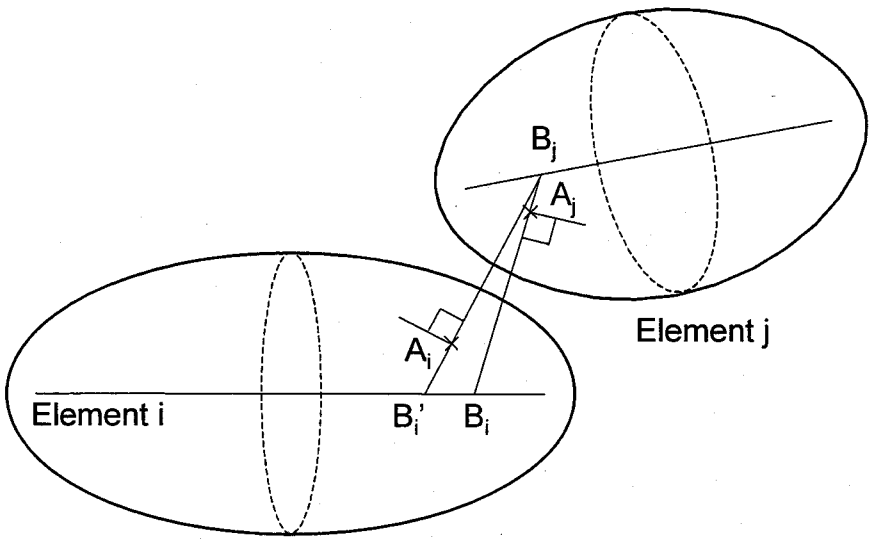

Fig. 4.2 Contact between ellipsoidal elements.

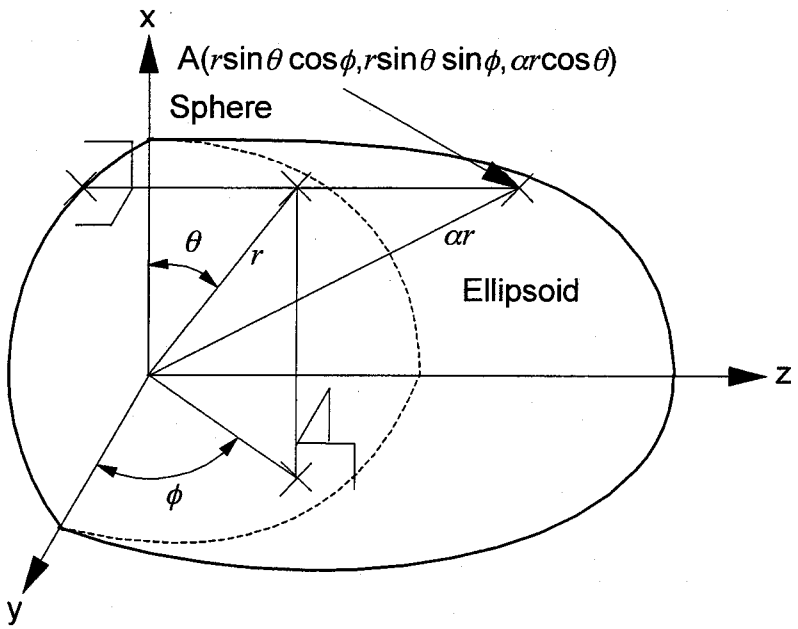

Fig. 4.3 Contact between ellipsoidal elements.

The variable ϕ in Equation (4.11) can be determined analytically on the plane including both point P and the major axis of the element. The variable θ is calculated by solving Equation (4.11) using the Newton-Raphson method and the normal through point P is obtained. A normal to element j through point B_i on the major axis of the element i is first obtained, and then intersection point B_j of the normal with the major axis of the element j is determined. Next, a normal to the element i through point B_j is determined and the intersection of the normal with the major axis of element i is point B_i'. The common normal is determined by repeating this procedure until convergence of θ. The overlap, δ, between the elements i and j is obtained by

$$\delta = \overline{A_iB_i} + \overline{A_jB_j} - \overline{B_iB_j}\,. \tag{4.15}$$

4.2.3 Contact Force and Moment

When the elements touch each other, the elastic repulsive forces in the normal and tangential directions at the contact point are applied. The unit normal vector, $\boldsymbol{n}$, at point A on the element surface is expressed using the normal vector, N, by

$$\boldsymbol{n} = \frac{N}{|N|} \tag{4.16}$$

$$N = \left(-A_x, -A_y, \frac{-A_z}{\alpha^2}\right). \tag{4.17}$$

The elastic repulsive force in the normal direction is calculated by

$$\boldsymbol{F}_{cn} = K_n \delta \boldsymbol{n} + C_n \Delta \boldsymbol{v}_n\,, \tag{4.18}$$

where K_n is the normal spring stiffness, C_n is the dumping modulus in the normal direction and $\Delta \boldsymbol{v}_n$ is the relative velocity vector between elements in the normal direction. In the tangential direction, both elastic repulsive and frictional forces are applied. The frictional force is calculated from the law of Coulomb friction. The tangential contact force is expressed as follows:

$$\boldsymbol{F}_{ct} = \begin{cases} \boldsymbol{F}_{ct}' & \left(|\boldsymbol{F}_{ct}'| < |\mu \boldsymbol{F}_{cn}|\right) \\ |\mu \boldsymbol{F}_{cn}| \dfrac{\boldsymbol{F}_{ct}'}{|\boldsymbol{F}_{ct}'|} & \left(|\boldsymbol{F}_{ct}'| \geq |\mu \boldsymbol{F}_{cn}|\right) \end{cases} \tag{4.19}$$

$$\boldsymbol{F}_{ct}' = K_t(\Delta \boldsymbol{v}_t \Delta t + \gamma) + C_t \Delta \boldsymbol{v}_t, \tag{4.20}$$

where μ is the coefficient of friction, K_t is the tangential spring stiffness, $\Delta \boldsymbol{v}_t$ is the relative velocity in the tangential direction, Δt is the time increment for a step, γ is the shear strain in the last step and C_t is the damping modulus in the tangential direction.

The contact moment, $\boldsymbol{M}$, is obtained from the normal and tangential contact forces as follows:

$$\boldsymbol{M} = \boldsymbol{L} \times (\boldsymbol{F}_{cn} + \boldsymbol{F}_{ct}), \tag{4.21}$$

where $\boldsymbol{L}$ is the position vector of the contact point in the local coordinate system. When an element touches more than two elements, all contact forces and moments are summed up as follows:

$$\boldsymbol{F}_c = \sum (\boldsymbol{F}_{cn} + \boldsymbol{F}_{ct}) \tag{4.22}$$

$$\boldsymbol{M}_c = \sum \boldsymbol{M}. \tag{4.23}$$

4.2.4 Viscous Force

When the grain moves in the liquid phase, the viscous force acts on the grain. The viscous force is approximated as that for the sphere having the same diameter to the length of the minor axis of the element as shown in Fig. 4.4;

$$\boldsymbol{F}_\ell = \frac{\ell}{2r} \boldsymbol{F}_{vs} \tag{4.24}$$

$$\boldsymbol{F}_{vs} = -6\pi \eta_\ell r \boldsymbol{v}, \tag{4.25}$$

where ℓ is the projection length shown in Fig. 4.4, $2r$ is the length of the minor axis of the element, η_ℓ is the coefficient of the viscosity of the liquid phase and $\boldsymbol{v}$ is the velocity vector of the element. Since the velocity and the angular velocity of elements are not large, the lift for the rotation is neglected in the present study.

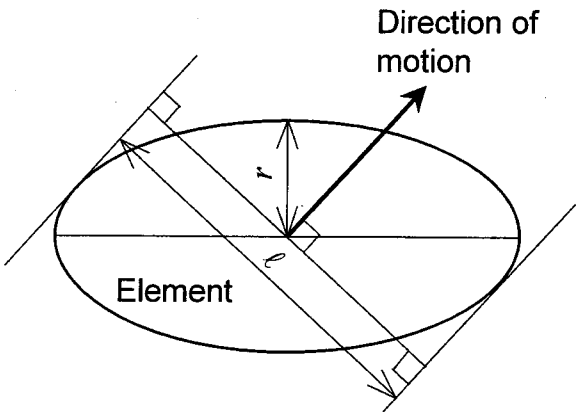

Fig. 4.4 Projection of ellipsoidal element onto plane perpendicular to motion of element.

4.3 Mushy-State Upsetting

4.3.1 Working Conditions

The mushy-state magnet is housed in a cylindrical capsule (made of mild steel) so as to avoid squeezing the liquid phase out. Its upsetting is shown in Fig. 4.5. The capsule is upset with two flat dies in the axial direction and the final reduction in height is 25%. The volume of the magnet is equal to that of the capsule.

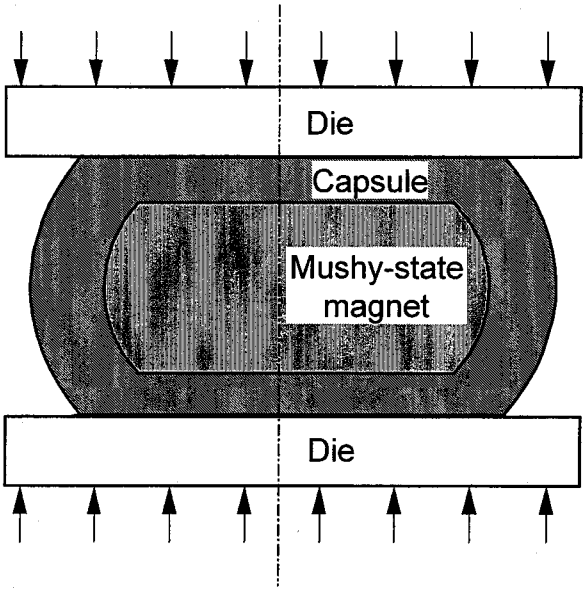

Fig. 4.5 Mushy-state upsetting.

4.3.2 Computation

The viscoplastic finite element method is employed to calculate the macroscopic plastic deformation of the capsule, and the microscopic motion of the grains in the mushy-state magnet is simulated by the distinct element method. Axi-symmetric deformation of the capsule is first calculated by the viscoplastic finite element method, and then the three-dimensional distinct element simulation is carried out using the calculated motion of the interface between the capsule and the magnet as a boundary condition.

The computational conditions used for the finite and the distinct element simulations are given in Table 4.1. To set the initial disposition of elements before the upsetting, the centres of the elements are located concentrically like hexagonal close-packed crystal structure of metals first, and the directions of the elements are randomly located while allowing overlap between elements. Then the distinct element simulation is continued without changing the shape of the interface between the capsule and magnet until a stable state has been reached. To stabilise the motion of the elements, the motion of all elements is stopped, *i.e.* the velocities of all elements are set for zero in every 50 steps.

To compare the two and three-dimensional simulations, the two-dimensional distinct element simulation using elliptical elements is performed. The three-dimensional simulation is performed under the same computational conditions as the two-dimensional simulation except a variation in the solid fraction and number of elements.

Table 4.1 Computational conditions used for finite and distinct element simulations of mushy-state plane-strain upsetting

Solid fraction ψ /%	30, 40 (3-D) 80 (2-D)
Grain aspect ratio α	1.67
Final reduction in height $\Delta h/h$ /%	25
Number of distinct elements n	293, 589, 921 (3-D) 148 (2-D)
Coefficient of friction between distinct element μ	0.1
Normal spring stiffness K_n /MN·mm^{-1}	65
Tangential spring stiffness K_t /MN·mm^{-1}	15
Density of solid phase /g·mm^{-3}	0.00786
Density of liquid phase ρ_ℓ /g·mm^{-3}	0.0069
Coefficient of viscosity η_ℓ /mPa·s	8
Flow stress of capsule (mild steel, 1000°C) /MPa	$\bar{\sigma} = 105\bar{\varepsilon}^{0.1}\dot{\bar{\varepsilon}}^{0.11}$
Coefficient of friction between die and capsule	0.25

4.3.3 Model Experiment

Since real rare-earth magnets are worked at about 1000°C, model materials are used in the experiment. The mushy-state magnet is modelled using acrylic resin grains and a Vaseline liquid phase, and the capsule is plasticine having similar deformation behaviour to hot steel. The grains are produced by casting acrylic resin into dies having ellipsoidal cavities. In the casting, solder bars are inserted at the major axis of the ellipsoid for one-third amount of grains. The capsule is upset with two flat dies using calcium carbonate as a lubricant. X-ray photographs are taken in the upsetting direction for every 5% reduction in height. Fig. 4.6 illustrates the X-ray images of the specimen in the model experiment for n=293 distinct elements and solid fraction ψ=40%. Only the image of the solder bars is obtained because X-ray easily passes through Vaseline but not solder. Since the length of all solder bars is known, the orientations of the acrylic resin grains are obtained from the measured length of solder bars in the image data.

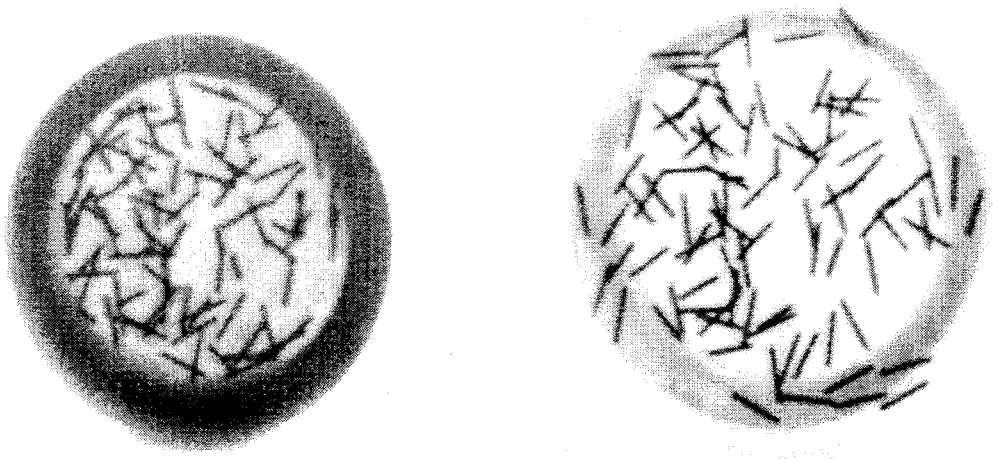

(a) $\Delta h/h$=0% (b) $\Delta h/h$=35%

Fig. 4.6 X-ray images of specimen in model experiment for n=293 and ψ=40%.

4.3.4 Evaluation of Degree of Grain Alignment

The direction of easy magnetisation in Pr-Fe-B magnets is located in the plane perpendicular to the major axis of the grain. By assuming that the intensity of magnetisation acts only in the direction perpendicular to the major axis, the component, H_{ui}, of the intensity of magnetisation in the upsetting direction for element i is expressed by

$$H_{ui} = H|\sin\varphi_i|, \tag{4.26}$$

where H is the intensity of magnetisation in the direction perpendicular to the major axis and φ_i is the angle between the major axis and the upsetting direction. The degree of grain alignment, A, for the magnet is defined by

$$A = \frac{1}{nH}\sum_{i=1}^{n} H_{ui}, \tag{4.27}$$

where n is the number of distinct elements. The degree of the grain alignment is 1 when the major axes of all the elements are perpendicular to the upsetting direction, whereas the degree is $\pi/4$=0.79 and $2/\pi$ =0.64 for the three and two-dimensional simulations in the fully random orientation, respectively.

4.4 Results

The calculated motion of grains in mushy-state upsetting for n=293 elements are illustrated in Fig. 4.7. The grains are mechanically aligned through local interactions with their neighbours. As the height is reduced, the grains are turned and the major axis of the grains is orientated perpendicular to the upsetting direction.

Calculated and experimental degrees of grain alignment for n=293 is plotted in Fig. 4.8. Although calculated and experimental degrees of grain alignment are different in the initial stage, the tendencies of variation are similar, and especially, the calculated and experimental results are in good agreement when the reduction is greater than 25%.

The variations of the degree of grain alignment with the reduction in height for the three-dimensional simulation of n=293 and the two-dimensional simulation of n=148 are plotted in Fig. 4.9. As the height is reduced, the degree of grain alignment increases. Although both tendencies of the three and the two-dimensional simulations

are similar, the value of degree of grain alignment for the three-dimensional simulation is larger than that for the two-dimensional one in early stages of upsetting, whereas the values are reversed at a 17% reduction. In the three-dimensional simulation, the solid fraction for the full packing and the degree of grain alignment in the random packing state are 0.74 and 0.79, respectively, whereas in the two-dimensional simulation, those values are 0.91 and 0.64. To simulate the motion of the grains, the use of the three-dimensional simulation is required.

The calculated distribution of the degree of grain alignment for n=293 and $\Delta h/h$=25% is shown in Fig 4.10. The degree of grain alignment is large near the centre of the magnet. Since elements near the interface between the capsule and the magnet are easy to move, the degree of grain alignment in the region near the interface is small.

The variations of the degree of grain alignment with the reduction in height for n=293, 589 and 921 are shown in Fig. 4.11. Although the initial disposition for n=293 is almost random orientation, those for n=589 and 921 are more or less aligned to the vertical direction. It is difficult to set the random orientation due to the anisotropy of shape for the ellipsoidal elements. Although the initial orientations have different values, the final degree of grain alignment is similar.

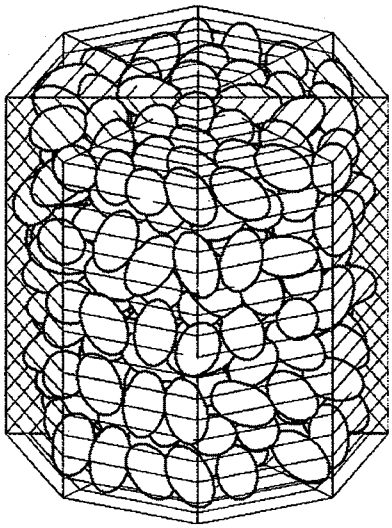

(a) $\Delta h/h$=0%

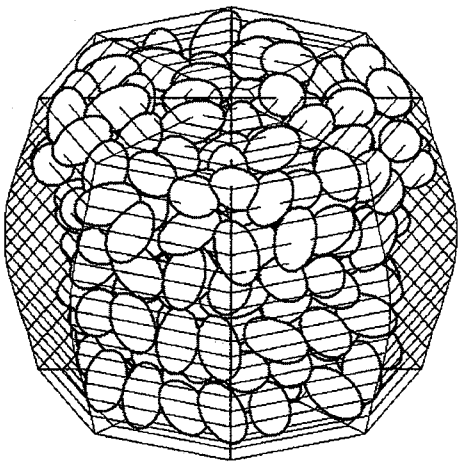

(b) $\Delta h/h$=15%

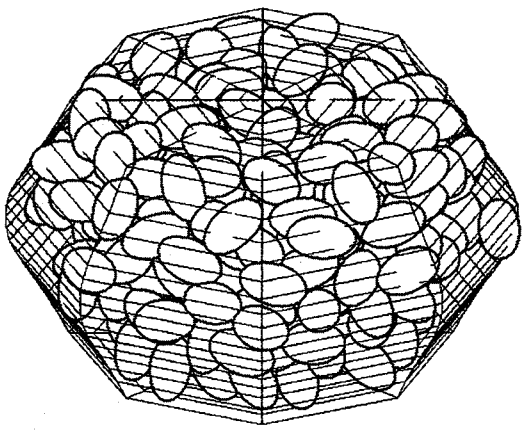

(c) $\Delta h/h$=25%

Fig. 4.7 Three-dimensional calculated motion of elements for n=293 and ψ=40%.

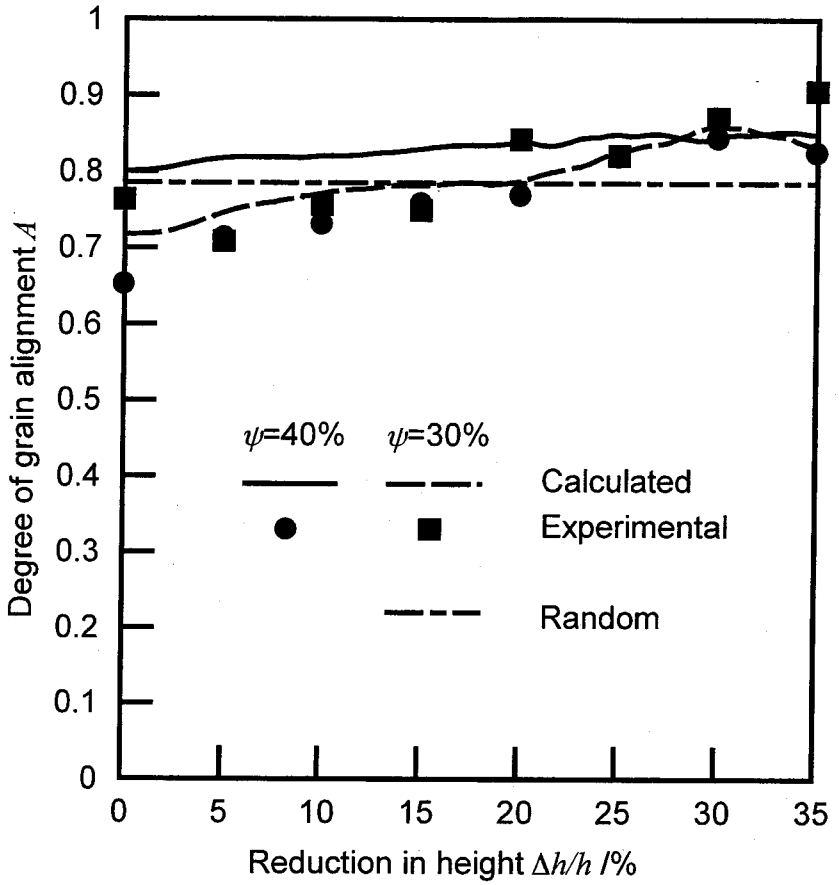

Fig. 4.8 Calculated and experimental degree of grain alignment for n=293.

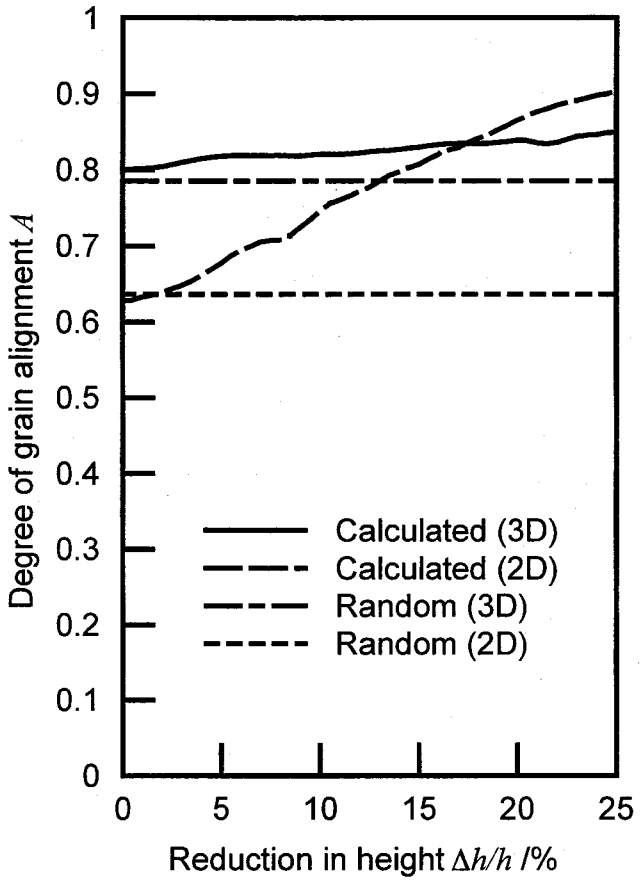

Fig. 4.9 Variation of degree of grain alignment with reduction in height in simulations for n=293 (3-D) and 148 (2-D), and ψ=40%.

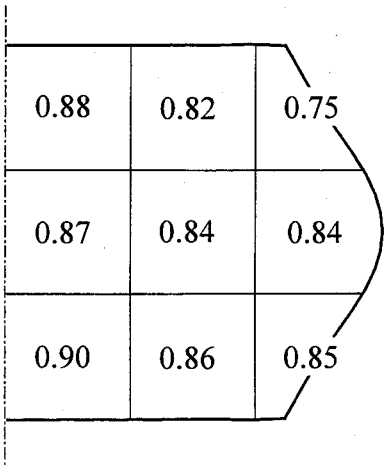

Fig. 4.10 Distribution of degree of grain alignment for n=293, ψ=40% and $\Delta h/h$=25%.

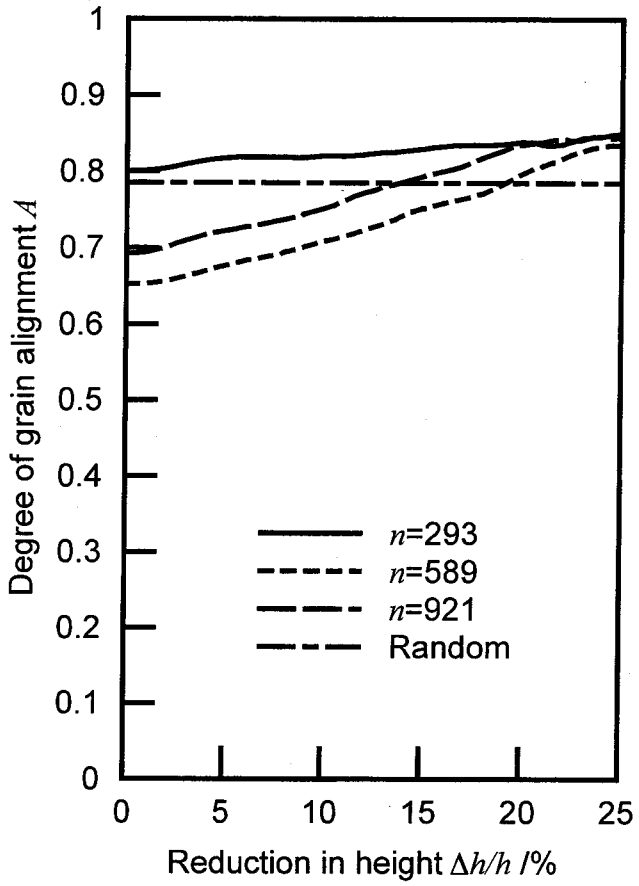

Fig. 4.11 Variation of degree of grain alignment with reduction in height for n=293, 589 and 921, and ψ=40%.

4.5 Conclusions

A three-dimensional distinct element method using ellipsoidal elements was proposed to simulate the three-dimensional motion of grains in mushy-state forming of magnets. Three-dimensional equations of motion and treatment of the contact were presented.

The calculated degree of grain alignment was in good agreement with the experimental one using a plasticine capsule, acrylic resin grains, and Vaseline liquid phase. The variation of the degree of grain alignment with the reduction in height was investigated. As the height decreased, the degree of grain alignment increased. The distribution of the degree of grain alignment was obtained and the degree of grain alignment was large near the centre of the magnet. In the case when the number of elements was larger than about 300, although the initial degrees of grain alignment were different, the final degrees were almost equal.

Since the grains in the rare-earth magnet are intermetallic compounds, the grains do not undergo plastic deformation in the early stages of forming. The grains, however, are deformed plastically as the forming progresses. It is desirable to develop a distinct element method taking the effect of plastic deformation of grains into account.

Although spherical elements have been used in most of the three-dimensional distinct element simulations for the sake of simplicity, real particles and grains are not spherical. The ellipsoidal elements have a wide range of application in the field of not only engineering but also science.

References

[1] T. Shimoda, K. Akioka, O. Kobayashi and T. Yamagami, High-energy cast Pr-Fe-B magnets, *J. Appl. Phys.*, **64** (1988), 5290-5292.

[2] T. Shimoda, K. Akioka, O. Kobayashi, T. Yamagami, T. Ohki, M. Miyagawa and T. Yuri, Hot-working behavior of cast Pr-Fe-B Magnets, *IEEE Trans. Magnetics*, **25**-5 (1989), 4099-4104.

[3] T. Shimoda, K. Akioka, O. Kobayashi and T. Yamagami, Hot-worked anisotropic Pr-Fe-B magnets, *Proc. 10th Int. Workshop on Rare-Earth Magnets and Their Application*, (1989), 389-398.

[4] T. Shimoda, K. Akioka, O. Kobayashi, T. Yamagami and A. Arai, Current situation in development of hot-rolled R-Fe-B magnet, *Proc. 11th Int. Workshop on Rare-Earth Magnets and Their Applications*, (1990), 17-28.

[5] P.A. Cundall, A computer model for simulating progressive, large-scale

movements in blocky rock systems, *Proc. Symp. Soc. Int. Rock Mech.*, Nancy **2**-8 (1971).

[6] P.A. Cundall and O.D.L. Strack, A discrete numerical model for granular assemblies, *Geotechnique*, **29** (1979), 47-65.

[7] K. Mori, M. Otsu, K. Osakada and M. Shiomi, Simulation of grain alignment in mushy-state forging of magnets by distinct element method, *Simulation of Materials Processing: Theory, Methods and Applications*, (Balkema, S.F. Shen and P. Dawson ed.), (1995), 1185-1190.

[8] M. Otsu, K. Mori, K. Osakada and M. Shiomi, Simulation of grain alignment in plane-strain forging of mushy-state magnets by distinct element and finite element methods, *Dynamic Plasticity and Structural Behaviors The 5th International Symposium on Plasticity and Its Current Applications*, (Gordon and Breach Publishers, S. Tanimura and A.S. Khan ed.), (1995), 297-300.

[9] M. Otsu, K. Mori and K. Osakada, Simulation of grain alignment in mushy-state forming of magnets by distinct element method, *JSME series A*, **62**-594 (1996), 452-457. (In Japanese)

[10] K. Mori, M. Otsu and K. Osakada, Distinct element simulation of grain alignment in mushy-state forging of magnets, *Int. J. Mech. Sci.*, **39**-7 (1997), 771-780.

[11] L. Rothenburg, Numerical simulation of idealized granular assemblies with plane elliptical particles, *Computers and Geotechnics*, **11** (1991), 315-329.

[12] J.M. Ting, M. Khwaja, L.R. Meachum and J.D. Rowell, An ellipse-based discrete element model for granular materials, *Int. J. Numer. Analyt. Meth. Geomechanics*, **17** (1993), 603-623.

[13] P.A. Cundall, Computer simulations of dense sphere assemblies, *Micromechanics of granular materials*, (Elsevier Science, M. Satake and J.T. Jenkins ed.), (1988), 113-123.

[14] S. Yamamoto and T. Matsuoka, A method for dynamic simulation of rigid and flexible fibers in a flow field, *J. Chem. Phys.*, **98** (1993), 644-650.

[15] J. Ghaboussi and R. Barbosa, Three-dimensional discrete element method for granular materials, *Int. J. Numer. Analyt. Meth. in Geomech.*, **14** (1990), 451-472.

CHAPTER 5

TWO-DIMENSIONAL DISTINCT ELEMENT SIMULATION OF MUSHY–STATE FORMING INCLUDING PRESSURE OF LIQUID PHASE

5.1 Introduction

In mushy-state forming, a heated metal is deformed under a mixture of solid and liquid phases. Since mushy-state forming has many advantages such as small working load and high mechanical properties of product compared with cast one, mushy-state forming has been recently applied to the production of automotive wheels made of an aluminium alloy [1].

In the early stages of mushy-state forging, only a part of a billet is in contact with dies and most of its surface is free. As the billet is compressed, liquid phase flows separately from solid phase. Since the squeezed liquid is concentrated at the surface layer, internal structure of the formed product in mushy state becomes heterogeneous. Although this heterogeneous distribution of internal structure is not desirable in most cases, it may be possible to utilise the distribution for functionally gradient materials. It is required to develop the technology for controlling the flow of liquid phase, and design billets and the forging process to obtain desired internal structure of the products [2].

In continuum mechanics such as the finite element method, however, the microscopic interaction between solid and liquid phases is neglected, *i.e.* macroscopic approach is taken. To simulate the microscopic behaviour on the scale of solid particles, the distinct element simulations for mushy-state forming are proposed in Chapter 2 and Chapter 4. These methods have been applied simulating the motion of grains in the mushy-state forming of rare-earth magnets. Since the magnet is contained in a steel capsule, the effect of pressure of liquid phase is neglected. In most mushy-state forming processes, however, workpieces heated to mushy state are directly deformed, and thus the effect of the pressure is not negligible.

In this chapter, the effect of pressure of liquid phase in mushy-state forming is introduced into the distinct element method to improve the accuracy of the calculated results. The solid particles are modelled as circular solid elements and liquid phase is

divided into triangular liquid elements having different pressure values. Plane-strain upsetting of a mushy-state billet is simulated and the distribution of pressure of liquid phase is investigated.

5.2 Method of Simulation

5.2.1 Modelling

Deformation behaviour of a mushy-state material strongly depends on solid fraction. The deformation of a high solid fraction material is induced by the interaction of solid particles, while that of a low solid fraction material is mainly caused by the flow of liquid phase. Since the flow of liquid phase results from local pressure gradient of liquid phase, it is very important to treat the pressure of liquid phase in the simulation of mushy-state forming. In this study, pressure of liquid phase is taken into account in the distinct element simulation. A model for the distinct element simulation of mushy-state forming including pressure of liquid phase is illustrated in Fig. 5.1. For the sake of simplicity, plane-strain deformation is treated. The grain of mushy-state material is modelled using circular solid element and the motion of the elements is calculated by the distinct element method. Liquid phase exists between grains and the distribution of pressure of liquid phase is calculated. The workpiece is divided into triangular liquid elements by connecting the centres of circular solid elements using the Delaunay triangulation [3], and pressure of liquid phase is evaluated at the centroid of the triangular liquid element. The pressure is obtained from the distribution of pressure around a moving cylinder in a viscous fluid. The effect of the change of pressure caused by the flow of liquid phase between neighbouring triangular liquid elements is also taken into consideration. The pressure of liquid phase and the frictional force between grain and liquid phase act on the grain.

The pressure of liquid phase caused by the motion of the grain is calculated first, and then the force acting on the grain is obtained by integrating the pressure on the surface of the grain. Next, the frictional force and the contact force between grains are calculated. All forces are summed up and the position and velocity of the grain are obtained by solving Newton's equations of motion.

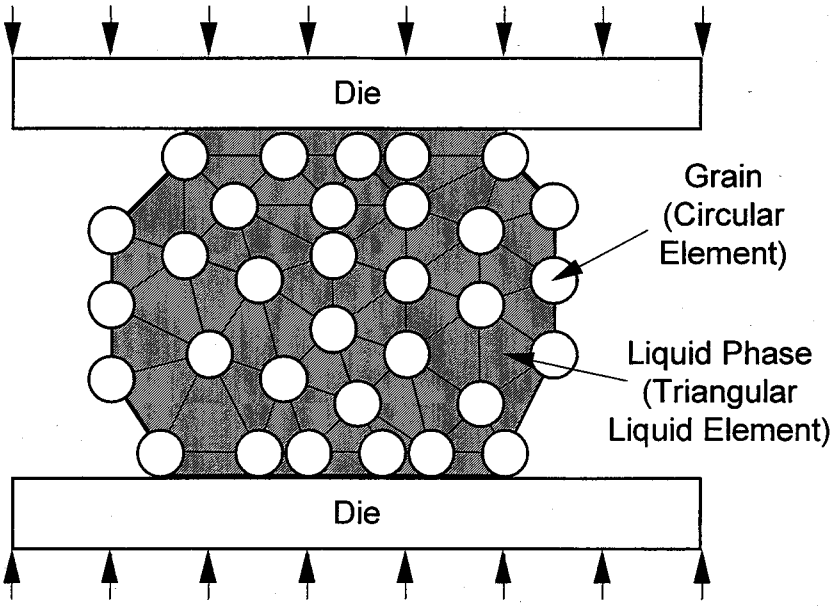

Fig. 5.1 Model for distinct element simulation of mushy-state forming including pressure of liquid phase.

5.2.2 Triangulation of Mushy-State Material

A mushy-state material is triangulated using the Delaunay triangulation by connecting the centroids of circular solid elements to calculate the pressure of liquid phase. In the Delaunay triangulation, a virtual triangle which contains the centroids of all circular solid elements inside is created. One circular solid element is selected and its centroid is connected to the vertexes of the virtual triangle, and then three new triangles are created. The next circular solid element is selected and the triangle which includes its centroid is searched. The centroid is connected to the vertexes of the found triangle and three new triangles are created. A tetragon created by joining two neighbouring triangles is considered. When the tetragon is convex, the common border of the two triangles is erased, the lengths of the two diagonals of the tetragon are compared, and the shorter one is selected. The other is removed and two new triangles are created. This process is repeated until all circular solid elements are used. Finally, the virtual triangle created in the first step is removed.

Since only convex polygons can be created by the Delaunay triangulation, when the area is slightly concave, long triangles are created at the border of the area. Since it is meaningless to evaluate the pressure of the long triangular liquid elements, long triangles having smaller angle than 10 degree or larger than 170 degree are erased.

5.2.3 Pressure of Liquid Phase

The pressure of the triangular liquid element is approximately obtained from the pressure distribution around a moving cylinder in a viscous fluid. A cylindrical coordinate system is considered. The origin is defined as the centre of the cylinder and the R-axis is the direction of the motion of the cylinder. The pressure at an arbitrary point, $P(R,\Theta)$, is expressed as follows [4]:

$$P(R,\Theta) = \frac{2\eta_\ell v}{\log\left(\frac{4\eta_\ell}{\rho_\ell r v}\right) - E + \frac{1}{2}} \cdot \frac{\cos\Theta}{R}, \tag{5.1}$$

where η_ℓ is the coefficient of viscosity of the liquid phase, v is the velocity of the cylinder, ρ_ℓ is the density of the liquid phase, r is the radius of the cylinder, and E is the Euler constant.

The pressure in the triangular liquid element is uniform. The pressure at the centroid of the triangular liquid element obtained from Equation (5.1) is added to that in the last step. A change in the pressure of the triangular liquid element caused by the flow between the neighbouring triangular liquid elements is illustrated in Fig. 5.2. P_i and S_i are the pressure and area of the triangular liquid element i, respectively. L_i is the width between the triangular liquid elements i and m. When the circular solid elements overlap each other, L_i is set for zero.

The pressure of the triangular liquid element m calculated from Equation (5.1) is set for P_m and the pressure after the change caused by the flow between the neighbouring triangular liquid elements, P_m'', is obtained as follows:

$$P_m'' = \frac{L_i P_i' + L_j P_j' + L_k P_k'}{L_i + L_j + L_k} + P_m \tag{5.2}$$

$$P_i' = \frac{S_i P_i + S_m P_m}{S_i + S_m}. \tag{5.3}$$

The pressures of the triangular liquid elements at the free surface are always set for atmospheric pressure.

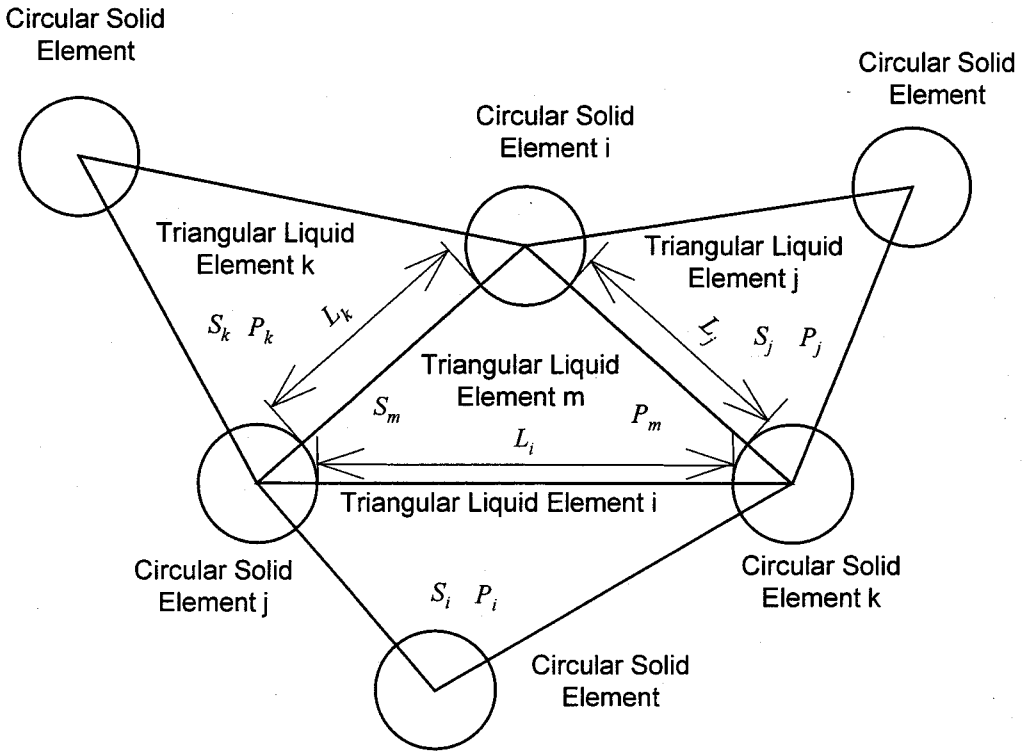

Fig. 5.2 Change of pressure of triangular liquid element caused by flow between neighbouring triangular liquid elements.

5.2.4 Formulation for Distinct Element Method

In the distinct element method, all forces acting on every circular solid element are summed up and Newton's equations of motion are solved. The acceleration of the circular solid element is obtained from the equation, and the velocity is calculated by integrating the acceleration. The position in the next step is obtained from the acceleration and velocity. Newton's equations of motion are expressed as follows:

$$\begin{cases} m\dot{\boldsymbol{v}} + \boldsymbol{F}_c + \boldsymbol{F}_f + \boldsymbol{F}_p = \boldsymbol{0} \\ I\dot{\omega} + M_c + M_f = 0, \end{cases} \tag{5.4}$$

where m and I are the mass and the moment of inertia of circular solid element, respectively. $\dot{\boldsymbol{v}}$ and $\dot{\omega}$ are the acceleration and the angular acceleration, respectively. $\boldsymbol{F}_c$ and M_c are the contact force and moment, and $\boldsymbol{F}_f$ and M_f are the frictional force and moment between circular solid element and liquid phase, respectively. $\boldsymbol{F}_p$ is the force induced from the pressure of the triangular liquid elements. Since the

translation velocity and the angular velocity of rotation are small, the lift that acts while a rotating object moves in a viscous fluid, is neglected. $\boldsymbol{F}_f$ and M_f are expressed [4] by

$$\boldsymbol{F}_f = -\frac{2\pi\eta_\ell \boldsymbol{v}}{\log\left(\frac{4\eta_\ell}{\rho_\ell r|\boldsymbol{v}|}\right) - E + \frac{1}{2}} \tag{5.5}$$

$$M_f = -4\pi\eta_\ell \omega r^2 . \tag{5.6}$$

The force induced from the pressure of liquid phase around the circular solid element is represented by

$$\boldsymbol{F}_p = P_m{}'' r\sqrt{2(1-\cos\kappa)}\boldsymbol{n}_p , \tag{5.7}$$

where κ is the central angle of the arc applied pressure of the triangular liquid element and $\boldsymbol{n}_p$ is the unit vector of the resultant force of the pressure as shown in Fig. 5.3.

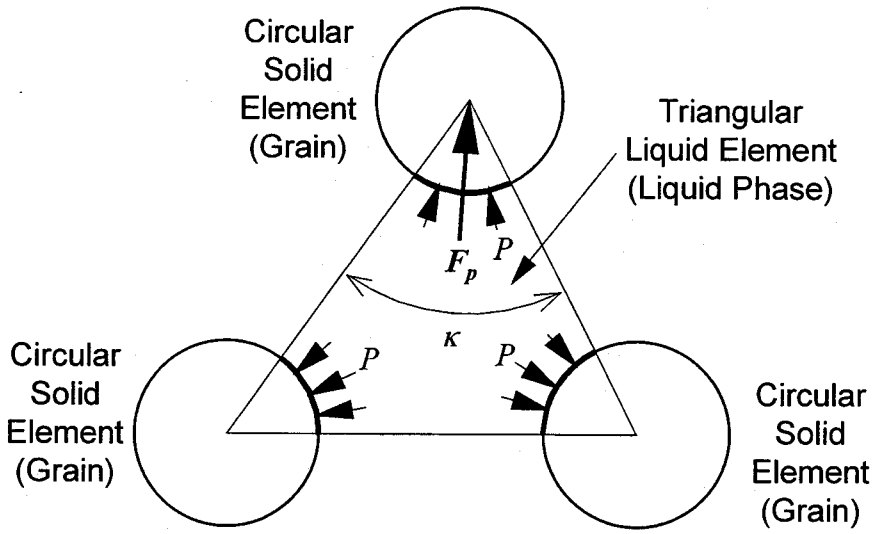

Fig. 5.3 Force induced from pressure of liquid phase.

5.3 Simulation of Mushy-State Upsetting

5.3.1 Computational Conditions

In this study, plane-strain mushy-state upsetting is treated. The shape of the workpiece is a square and two flat dies are used. The lower die is fixed and the upper one is moved downward at a constant velocity. Computational conditions used for simulation of mushy-state upsetting are given in Table 5.1.

Table 5.1 Computational conditions used for simulation of mushy-state upsetting.

Solid fraction ψ /%	65
Final reduction in height $\Delta h/h$ /%	15
Number of distinct elements n	314
Coefficient of friction between circular solid elements μ	0.1
Normal spring stiffness K_n /MN·mm^{-1}	65
Tangential spring stiffness K_t /MN·mm^{-1}	15
Density of solid phase /g·mm^{-3}	0.00786
Density of liquid phase ρ_ℓ /g·mm^{-3}	0.0069
Coefficient of viscosity η_ℓ /mPa·s	8
Ratio of height of billet to width	1

5.3.2 Results

The calculated motion of grains in mushy-state upsetting is shown in Fig. 5.4. In the initial state, the number of triangular liquid elements is 570 and it increases as the height is reduced, because the disposition of circular solid elements becomes irregular and the number of triangular liquid elements sharing same circular solid element increases at the deformed surface. For the reduction in height $\Delta h/h$=15%, the lower part of the workpiece is not deformed yet and the circular solid elements are aligned regularly, while the upper part is deformed and the distances between circular solid elements are reduced. The solid fraction of the upper part of the free surface is low. Shear bands are observed in the central part.

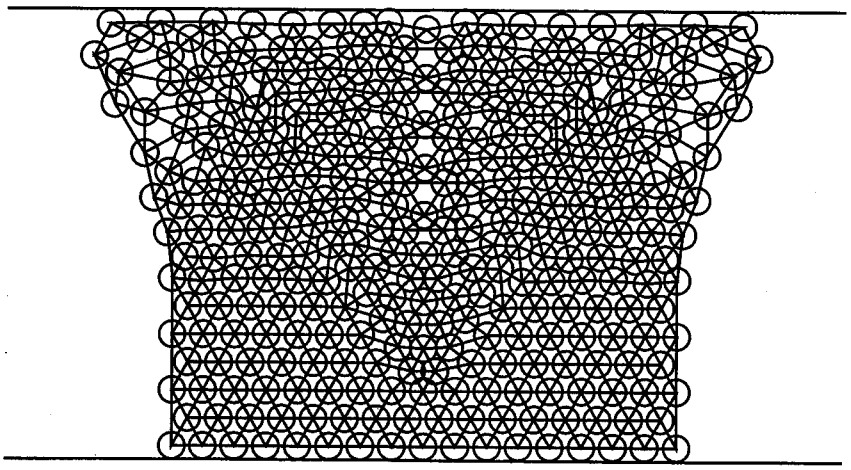

Fig. 5.4 Calculated motion of grains in mushy-state upsetting for $\Delta h/h$=15%.

The calculated distribution of the pressure of liquid phase for $\Delta h/h$=15% is illustrated in Fig. 5.5. Compressive pressure (positive value) occurs along the shear bands, and expansive pressure (negative value) is distributed in the upper central part and near the free surface because the circular solid elements move toward the outer side. Although the pressure in the upper central part is compressive in the early stages, it becomes expansive after the circular solid elements come to touch each other. Since the condition of volume constancy is not taken into account, the circular solid elements near the free surface shatter when the reduction becomes larger.

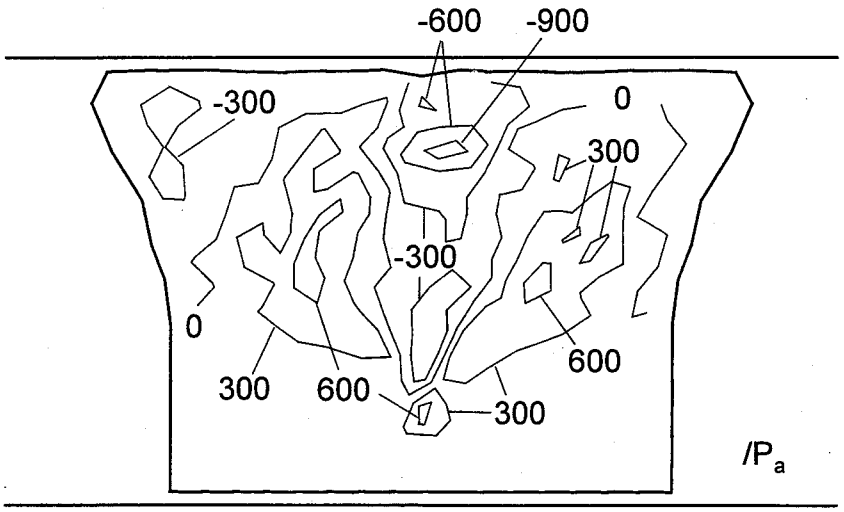

Fig. 5.5 Calculated distribution of pressure of liquid phase for $\Delta h/h$=15%.

5.4 Conclusions

Deformation behaviour of a mushy-state material strongly depends on solid fraction. The deformation of a low solid fraction material is mainly caused by the flow of liquid phase. Since the flow of liquid phase results from local pressure gradient of liquid phase, it is very important to treat the pressure of liquid phase. In this study, the effect of the pressure of liquid phase was introduced into the distinct element simulation for mushy-state forming. Simulation of mushy-state upsetting was performed and compressive pressure along the shear bands was observed. The problem of handling the condition of volume constancy remains.

Although a two-dimensional simulation was performed, the deformation behaviours result from two and three-dimensional simulations are different. It is desirable to develop a three-dimensional method.

References

[1] *Nikkei New Materials*, **6** (1992), 10-23. (In Japanese)

[2] M. Kiuchi, *Proc. 165th Japanese Symp. Technol. Plastisity*, (1995), 1-14. (In Japanese)

[3] T. Taniguchi, Automatic mesh generation, (1992), *Morikita Press*. (In Japanese)

[4] I. Imai, Fluid dynamics, **1** (1973), *Syokabo*. (In Japanese)

CHAPTER 6

THREE-DIMENSIONAL DISTINCT ELEMENT SIMULATION OF MUSHY–STATE FORMING INCLUDING PRESSURE OF LIQUID PHASE

6.1 Introduction

In mushy-state forming, a heated metal is deformed under a mixture of solid and liquid phases. In the early stages of mushy-state forging, only a part of a billet is in contact with dies and most of its surface is free. As the billet is compressed, liquid phase flows separately from solid phase. Since the squeezed liquid is concentrated at the surface layer, internal structure of the formed product in mushy state becomes heterogeneous. Although this heterogeneous distribution of internal structure is not desirable in most cases, it may be possible to utilise the distribution for functionally gradient materials. It is required to develop the technology for controlling the flow of liquid phase, and design billets and the forging process to obtain desired internal structure of products [2].

In continuum mechanics such as the finite element method, however, the microscopic interaction between solid and liquid phases is neglected, *i.e.* macroscopic approach is taken. The two-dimensional distinct element simulation of mushy-state forming including pressure of liquid phase is proposed in Chapter 5. Since the behaviour of grains calculated by the two-dimensional method is more or less different from that for the actual forming process, it is desirable to develop a three-dimensional method for simulating the motion of grain in mushy-state forming.

In this chapter, three-dimensional distinct element simulation of mushy-state forming including pressure of liquid phase is presented. The solid particles are modelled as spherical solid elements and the liquid phase is divided into tetrahedral liquid elements having different pressure values. Axi-symmetric upsetting of a cylindrical mushy-state billet is simulated and the distribution of solid fraction is investigated.

6.2 Method of Simulation

6.2.1 Modelling

Deformation behaviour of mushy-state materials strongly depends on solid fraction. The deformation of a high solid fraction material is induced by the interaction of solid particles, while, that of a low solid fraction material is mainly caused by the flow of liquid phase. Since the flow of liquid phase results from local pressure gradient of liquid phase, it is very important to treat the pressure of liquid phase in the simulation of mushy-state forming. In this study, the method proposed in Chapter 5 is expanded to the three-dimensional one and pressure of liquid phase is taken into account in the three-dimensional distinct element simulation. A model for the distinct element simulation of mushy-state forming including pressure of liquid phase is illustrated in Fig. 6.1. The grains of mushy-state material is modelled using spherical solid elements and the motion of the elements is calculated by the distinct element method. Liquid phase exists between grains and the distribution of pressure of liquid phase is calculated. The workpiece is divided into tetrahedral liquid elements by connecting the centres of spherical solid element using the three-dimensional Delaunay triangulation [3], and pressure of liquid phase is evaluated at the centroid of the tetrahedral liquid element. The pressure is obtained from the distribution of pressure around a moving sphere in a viscous fluid. The effect of the change of pressure caused by the flow of liquid phase between the neighbouring tetrahedral liquid elements is also taken into consideration. The pressure of liquid phase and the frictional force between grain and liquid phase act on the grain.

The pressure of liquid phase caused by the motion of the grain is calculated first, and then the force acting on the grain is obtained by integrating the pressure on the surface of the grain. Next, the frictional force and the contact force between grains are calculated. All forces are summed up and the position and velocity of the grain are obtained by solving Newton's equations of motion.

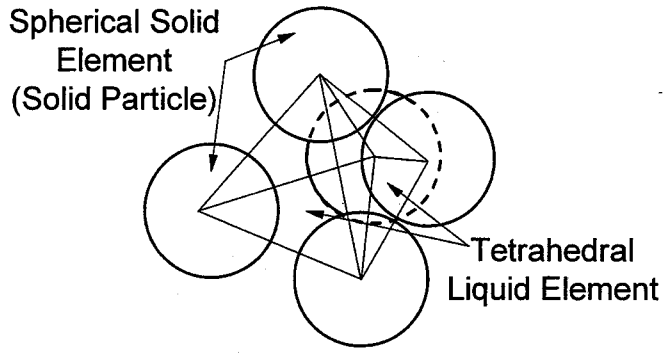

Fig. 6.1 Model for distinct element simulation of mushy-state forming including pressure of liquid phase.

6.2.2 Triangulation of Mushy-State Material

A mushy-state material is triangulated using the three-dimensional Delaunay triangulation by connecting the centroids of the spherical solid elements to calculate pressure of liquid phase. In the Delaunay triangulation, a virtual tetrahedron which contains the centroids of all spherical solid elements is created. One spherical solid element is selected and its centroid is connected to the vertexes of the virtual tetrahedron, and then four new tetrahedra are created. The next spherical solid element is selected and the tetrahedron which includes its centroid is searched. The centroid is tested to determine which circumsphere of the adjacent tetrahedra to the found tetrahedron. A polyhedron is created by associating the all tetrahedra which circumspheres include the centroid, and the tetrahedra are removed. New tetrahedra are created by connecting the centroid to all triangular facets on the surface of the polyhedron. This process is repeated until all spherical solid elements have been used. Finally, the virtual tetrahedron created in the first step is erased.

Since only convex polyhedra can be created by the three-dimensional Delaunay triangulation, when the area is slightly concave, long tetrahedra are created at the border of the area. Since it is meaningless to evaluate pressure of the long tetrahedral liquid elements, long tetrahedra are removed. Long tetrahedra are determined as follows. The height ratio of the tetrahedron in question and that of the right tetrahedron having the same volume as it are calculated. When the height ratio is larger than 10 or smaller than 0.1, the tetrahedron is removed.

6.2.3 Pressure of Liquid Phase

The pressure of the tetrahedral liquid element is approximately obtained from the pressure distribution around a moving sphere in a viscous fluid. A spherical coordinate system is considered. The origin is defined as the centre of the cylinder and the R-axis is the direction of the motion of the sphere. The pressure at an arbitrary point, $P(R,\Theta)$, is calculated from Stokes' approximation as follows [4]:

$$P(R,\Theta) = -\frac{3}{2}\cdot\frac{\eta_\ell r|\boldsymbol{v}|}{R^2}\cos\Theta\,, \tag{6.1}$$

where η_ℓ is the coefficient of viscosity of the liquid phase, $\boldsymbol{v}$ is the velocity of the sphere and r is the radius of the sphere.

The pressure in the tetrahedral liquid element is uniform. The pressure at the centroid of the tetrahedral liquid element obtained from Equation (6.1) is added to it in the last step. A change in the pressure of the tetrahedral liquid element caused by the flow between the neighbouring tetrahedral liquid elements is illustrated in Fig. 6.2. P_i and V_i are the pressure and the volume of the tetrahedral liquid element i, respectively. S_i is the area between the tetrahedral liquid elements i and m. When the spherical solid elements overlap each other and the value of S_i becomes negative, S_i is set for zero.

The pressure of the tetrahedral liquid element m calculated from Equation (6.1) is set for P_m and the pressure after the change caused by the flow between the neighbouring tetrahedral liquid elements, P_m'', is obtained as follows:

$$P_m'' = \frac{S_iP_i'+S_jP_j'+S_kP_k'+S_lP_l'}{S_i+S_j+S_k+S_l} + P_m \tag{6.2}$$

$$P_i' = \frac{V_iP_i+V_mP_m}{V_i+V_m}\,. \tag{6.3}$$

The pressures of the tetrahedral liquid elements at the free surface are always set for atmospheric pressure.

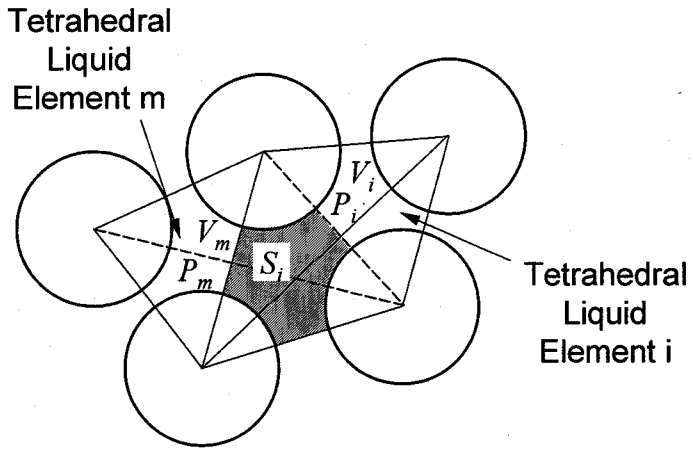

Fig. 6.2 Change of pressure of triangular liquid element caused by flow between neighbouring tetrahedral liquid elements.

6.2.4 Formulation for Distinct Element Method

In the distinct element method, all forces acting on every spherical solid element are summed up and Newton's equations of motion are solved. The acceleration of the spherical solid element is obtained from the equation, and the velocity is calculated by integrating the acceleration. The position in the next step is obtained from the acceleration and velocity. Newton's equations of motion are expressed as follows:

$$\begin{cases} m\dot{\boldsymbol{v}} + \boldsymbol{F}_c + \boldsymbol{F}_f + \boldsymbol{F}_p = \boldsymbol{0} \\ I\dot{\boldsymbol{\omega}} + \boldsymbol{M}_c + \boldsymbol{M}_f = \boldsymbol{0}, \end{cases} \tag{6.4}$$

where m and I are the mass and the moment of inertia of the spherical solid element, respectively. $\dot{\boldsymbol{v}}$ and $\dot{\boldsymbol{\omega}}$ are the acceleration and the angular acceleration, respectively. $\boldsymbol{F}_c$ and $\boldsymbol{M}_c$ are the contact force and moment, and $\boldsymbol{F}_f$ and $\boldsymbol{M}_f$ are the frictional force and moment between spherical solid element and liquid phase, respectively. $\boldsymbol{F}_p$ is the force induced from the pressure of the tetrahedral liquid elements. Since the translation velocity and the angular velocity of rotation are small, the lift that acts while a rotating object moves in a viscous fluid, is neglected. $\boldsymbol{F}_f$ and $\boldsymbol{M}_f$ are expressed [4] by

$$\boldsymbol{F}_f = -4\pi\eta_\ell r\boldsymbol{v} \tag{6.5}$$

$$\boldsymbol{M}_f = -8\pi\eta_\ell r^3\boldsymbol{\omega}\,. \tag{6.6}$$

The force induced from the pressure of liquid phase around the spherical solid element is represented by

$$\boldsymbol{F}_p = \int_S P\boldsymbol{n}dS, \tag{6.7}$$

where $\boldsymbol{n}$ is the unit vector of the resultant force of the pressure as shown in Fig. 6.3.

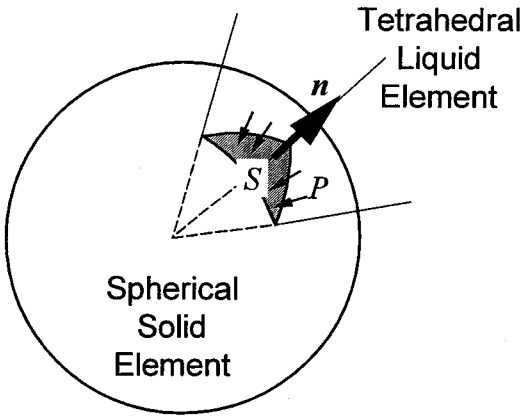

Fig. 6.3 Force induced from pressure of liquid phase.

6.3 Simulation of Mushy-State Upsetting

6.3.1 Computational Conditions

In this study, axi-symmetrical mushy-state upsetting is considered. The shape of the workpiece is cylindrical and two flat dies are used. The lower die is fixed and the upper one is moved downward at a constant velocity. Computational conditions used for simulation of mushy-state upsetting are given in Table 6.1.

6.3.2 Results

The calculated motion of grains in mushy-state upsetting is shown in Fig. 6.4. In the initial state, the number of tetrahedral liquid elements is 1662 and the number increases as the height is reduced and it is 1894 in the final state. Most of the calculating time is taken for the Delaunay triangulation process. Since the condition of volume constancy is not taken into account, the spherical solid elements near the free surface shatter when the reduction becomes larger. Consequently, the final volume is about 2.3 times as large as the initial one.

The calculated distribution of solid fraction for $\Delta h/h$=50% is illustrated in Fig. 6.5. Solid fraction is high near the symmetrical axis and low at the free surface.

Table 6.1 Computational conditions used for simulation of mushy-state upsetting.

Solid fraction ψ /%	57
Final reduction in height $\Delta h/h$ /%	50
Number of distinct elements n	357
Coefficient of friction between spherical solid elements μ	0.1
Normal spring stiffness K_n /MN·mm^{-1}	65
Tangential spring stiffness K_t /MN·mm^{-1}	15
Density of solid phase /g·mm^{-3}	0.00786
Density of liquid phase ρ_ℓ /g·mm^{-3}	0.0069
Coefficient of viscosity η_ℓ /mPa·s	8

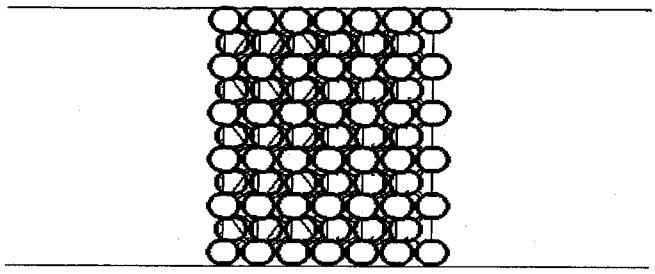

(a) $\Delta h/h$=0%

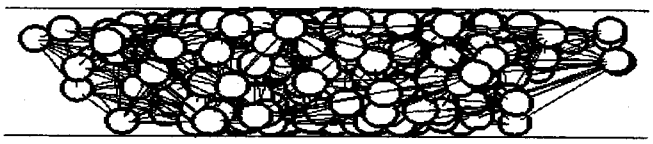

(b) $\Delta h/h$=50%

Fig. 6.4 Calculated motion of grains in mushy-state upsetting.

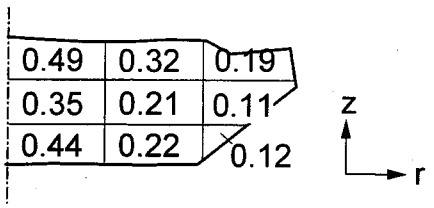

Fig. 6.5 Calculated distribution of solid fraction for $\Delta h/h$=50%.

6.4 Conclusions

The effect of pressure of liquid phase is introduced into the three-dimensional distinct element simulation for mushy-state forming. Simulation of axi-symmetrical mushy-state upsetting is performed and the distribution of solid fraction is calculated. Since most of the calculating time is taken for the Delaunay triangulation process, it is necessary to improve the algorithm for triangulation. The problem of taking the condition of volume constancy into account remains.

References

[1] *Nikkei New Materials*, **6** (1992), 10-23. (In Japanese)

[2] M. Kiuchi, *Proc. 165th Japanese Symp. Technol. Plastisity*, (1995), 1-14. (In Japanese)

[3] H. Borouchaki and S.H. Lo, Fast Delaunay triangulation in three dimensions, *Comp. Meth. Appl. Mech. Eng.*, **128** (1995), 153-167.

[4] I. Imai, Fluid dynamics, **1** (1973), *Syokabo*. (In Japanese)

CHAPTER 7

CONCLUDING REMARKS

7.1 Summary

7.1.1 Two-Dimensional Grain Alignment of Mushy-State Magnet

The distinct element simulation of grain alignment of rare-earth magnet in mushy-state forging is performed. Since the alignment is caused by the shape of grain, elliptical elements are used in the simulation. The procedure of detecting contact for elliptical elements is proposed. The effect of the liquid phase is treated as the viscous resistant force. The degree of grain alignment increases as the height is decreased. The increase in grain alignment is large, up to a 30% reduction, and then the alignment is saturated. The calculated degree of grain alignment is in good agreement with the experimental one using a plasticine capsule, acrylic resin grains and Vaseline liquid phase. Although the degree of grain alignment increases with the solid fraction, the degree is almost constant in the solid fraction above 80%. The degree of grain alignment increases as the aspect ratio increases. The distribution of grain alignment is also investigated. The degree of grain alignment is large near the centre of the magnet, while that is small at the sides.

7.1.2 Optimum Working Condition

The simulation method proposed in Chapter 2 is applied to decide the optimum working conditions for the mushy-state forging of rare-earth magnet. In the optimisation of the working conditions, the degree of grain alignment and crop loss are evaluated. First, the volume rate of the capsule and the die angle are fixed and the aspect ratio of the magnet is optimised. Next, the volume rate of the capsule is optimised using the fixed die angle and the optimised aspect ratio of the magnet. Finally, the die angle is optimised with the optimised aspect ratio of the magnet and volume rate of the capsule.

The aspect ratio of the magnet, the volume rate of the capsule and the die angle are determined to be 0.67, 30% and 1°, respectively. To compare with the case in which the aspect ratio of the magnet, the volume rate of the capsule and the die angle are 0.33, 50% and 0°, respectively, the degree of grain alignment and the crop loss are improved 2.9% and 8.9%, respectively.

7.1.3 Three-Dimensional Grain Alignment of Mushy-State Magnet

The simulation method proposed in Chapter 2 is expanded to three dimensions and the three-dimensional distinct element method using ellipsoidal elements is proposed. The procedure of detecting contact for ellipsoidal elements is represented. The calculated degree of grain alignment is in good agreement with the experimental one using a plasticine capsule, acrylic resin grains, and Vaseline liquid phase. The variations of the degree of grain alignment with the reduction in height for the three-dimensional simulation are compared with that for the two-dimensional one. As the height decreases, the degree of grain alignment increases. Although the tendencies of both the three and two-dimensional simulations are similar, the value of the degree of grain alignment for the three-dimensional simulation is larger than that of the two-dimensional one in early stages of upsetting, whereas the values are reversed in the later stages. The distribution of the degree of grain alignment is obtained and the degree of grain alignment is large near the centre of the magnet. The effect of the number of elements on the variations of the degree of grain alignment with the reduction in height is investigated. In the case when the number of elements is larger than about 300, although the initial degrees of grain alignment are different, the final degrees are almost equal.

7.1.4 Two-Dimensional Distinct Element Simulation of Mushy-State Forming Including Pressure of Liquid Phase

The two-dimensional distinct element method including the pressure of the liquid phase is proposed. The grains are modelled as circular solid element and pressure of liquid phase is calculated at the centres of the triangular liquid elements. The

triangular liquid elements are created by connecting the centre of the circular solid element using the Delaunay triangulation. In the simulation of mushy-state upsetting, the shear bands are observed and the pressure of liquid phase is high near the shear band.

7.1.5 Three-Dimensional Distinct Element Simulation of Mushy-State Forming Including Pressure of Liquid Phase

The simulation method presented in Chapter 5 is expanded to three dimensions. The grains are modelled using spherical solid elements and the pressure of liquid phase is calculated at the centres of the tetrahedral liquid element. The tetrahedral liquid elements are created by connecting the centres of the spherical solid elements using the three-dimensional Delaunay triangulation. The distribution of solid fraction in axi-symmetrical mushy-state upsetting is obtained and solid fraction is high near the symmetrical axis and low at the free surface.

7.2 Further Prospects

7.2.1 Simulation of Grain Alignment of Mushy-State Magnet

The grains are treated not to undergo plastic deformation but it is possible to occur plastic deformation in forming. It is desired to take plastic deformation of the grains into account for the distinct element method.

Magnetic property of products is roughly approximated and evaluated by degree of grain alignment in this study. If the magnetic properties were evaluated more accurately in the simulation, the simulation would be more useful tool to design forming process.

7.2.2 Distinct Element Simulation of Mushy-State Forming Including Pressure of Liquid Phase

In the distinct element simulation, the motion of elements is calculated by the interaction of the elements. In mushy-state forming in low solid fraction, deformation

behaviour depends on not the interaction of grains but the flow of liquid component. Since pressure of liquid phase is roughly calculated in this study, it is necessary to calculate the flow of liquid phase more accurately, *e.g.* the condition of volume constancy of liquid phase, distribution of pressure and flow front at the free surface.

7.2.3 Distinct Element Simulation for Forming

Although the distinct element method is a powerful tool to handle microscopic factors such as the size, shape and distribution of particles, it is difficult to calculate plastic deformation of particles and working load quantitatively because the simple spring-dashpot model is employed. It is desired to develop new models that can treat the force between particles accurately.

In the distinct element method, each particle is modelled as element and it is impossible to treat actual number of particles. It is desired to combine microscopic method and macroscopic one.